

# Title in progress

G. I. Perren<sup>1,2</sup>, E. E. Giorgi<sup>1</sup>, A. Moitinho<sup>3</sup>, G. Carraro<sup>4</sup>, M. S. Pera<sup>2</sup>, and R. A. Vázquez<sup>1,2</sup>

<sup>1</sup> Facultad de Ciencias Astronómicas y Geofísicas (UNLP), IALP-CONICET, 1900 La Plata, Argentina  
e-mail: gabrielperren@gmail.com

<sup>2</sup> Consejo Nacional de Investigaciones Científicas y Técnicas (CONICET), Buenos Aires, Argentina

<sup>3</sup> SIM, Faculdade de Ciências, Universidade de Lisboa, Ed. C8, Campo Grande, P-1749-016 Lisboa, Portugal

<sup>4</sup> Dipartimento di Fisica Astronomia Galileo Galilei, Vicolo Osservatorio 3, Padova, I-35122, Italy

Received June 15, 2019; accepted September 16, 2019

## ABSTRACT

**Aims.** To analyze sixteen faint and unknown open clusters placed along the Milky Way plane in a sector extending from  $290^\circ$  to  $320^\circ$  in galactic longitude.

**Methods.** We have carried out an *UBVI* photometric study on all clusters. The photometric observations were analyzed in an automatic way in order to get a homogeneous set of results regarding distance, reddening, mass, age and metallicity for each individual cluster. Distances obtained from the photometric analysis were compared to those estimated using parallax data from the Gaia satellite 2<sup>nd</sup> data release (Gaia DR2), through a Bayesian analysis.

**Results.** We have found that only eight out of the sixteen clusters are real entities and another two remain categorized as probable open clusters. The rest of them in the sample are most probably random stellar fluctuations. The comparison of distances coming from the photometric analysis and from Gaia data for these ten clusters has yielded a variable level of disagreement. Applying various suggested systematic zero point corrections for Gaia DR2 parallax data from recent literature, tends to improve the results. We draw attention to the importance of the use in this article of the *U-B* index which allows us to perform a realistic estimate of the reddening for each cluster and therefore of the visual absorption, which is a critical parameter for obtaining a more accurate distance determination when using photometric methods.

**Conclusions.** We found that in the case of robust open clusters such as NGC 4349 and Trumpler 13 distances from both methods tend to be coincident (**is this still true?**). As for the contribution of the present sample to the knowledge of the spiral structure nearby to the Sun, we found just three objects which are young enough as to be assumed potential spiral arm components located not far from the Carina feature.

**Key words.** Methods: statistical – Galaxies: star clusters: general – (Galaxy:) open clusters and associations: general – Techniques: photometric

## 1. Introduction

Galactic open clusters are routinely used as probes of the structure and evolution of the Milky Way disk. Their fundamental parameters, like age, distance, and metallicity allow us to define the large scale structure of the disk and to cast light on its origin and assembly (Janes & Adler 1982; Moitinho 2010; Cantat-Gaudin et al. 2018). Young open clusters can be used to trace spiral arms and star forming regions (Moitinho et al. 2006; Vázquez et al. 2008), while older clusters are better probes of the chemical evolution of the thin disk (Magrini et al. 2009). The recent second release of Gaia satellite data (Gaia Collaboration et al. 2018) is producing a tremendous advance in the study of the Galactic disk and its star cluster population.

Basic parameters for a large number of clusters are now available with unprecedented accuracy (Cantat-Gaudin et al. 2018; Soubiran et al. 2018; Bossini et al. 2019). Proper motions may be employed to select cluster members and parallaxes can be used to derive distances. It comes to happen that in some cases Gaia based distances strongly disagree with photometric or spectrophotometric distances. Nonetheless, for reasonably short distances the two different methods yield similar results within the uncertainties (Cantat-Gaudin et al. 2018). At larger distances Gaia photometry is of poorer quality than the more traditional ground based photometry, and accurate parallaxes are not avail-

able or possible for the moment. It is difficult to say which the critical distance is, since it also depends on the interstellar absorption and the crowding of a given star cluster. In all cases it is necessary to count on cleaner color-color and color-magnitude diagrams.

In this work we put together a sample of previously unstudied star clusters located at different distances for which we provide CCD *UBVI* photometry, and complement with data available from Gaia DR2. The purpose of this investigation is twofold. Firstly, we wanted to study Galactic structure in a poorly known Galactic sector, located at approximately  $270^\circ < l < 300^\circ$ . In this region one would expect to be able to follow the Perseus arm coming out of the third Galactic quadrant. On the contrary, no stellar traces have been detected so far for this arm, which is so prominent in the second quadrant, and clearly visible also in the third. The sample of clusters originally selected for this purpose and analyzed in this paper is shown in Table 1 together with their absolute coordinates referred to the J2000.0 equinox and also the galactic ones. However, this proved quite a difficult task, since in that specific sector extinction is particularly strong, and variable. This makes it cumbersome not only to derive solid basic parameters, but, even worse, to establish if a visual stellar aggregate is a physical cluster or simply a random enhancement of field stars produced

by patchy reddening. Secondly, Gaia DR2 offers us a possible way out. In fact, we can use Gaia data to make our analysis more robust by combining our *UBVI* CCD data with Gaia DR2 (*G* magnitude, parallax, and proper motions). For these reasons we employed the Automated Stellar Cluster Analysis code (ASteCA; Perren et al. 2015) to derive clusters' fundamental parameters from *G-UBVI* data, and a Bayesian technique to extract membership and distances from Gaia DR2.

The layout of the paper is as follows: in Section 2 we present the cluster sample indicating their positions in the Galaxy. Section 3 is devoted to explain the observations and the reduction process of photometry. In Section 4 we describe the tools to analyze the photometric data and the method to connect Gaia DR2 with photometric results. A cluster by cluster report of the results obtained is presented in Section 5. In Section 6 three different possible offsets to Gaia DR2 parallax data are applied and discussed. Conclusions of the paper are given in Section 7.

## 2. The cluster sample

Table 1 shows equatorial coordinates ( $\alpha$ ,  $\delta$ ) and galactic coordinates ( $l$ ,  $b$ ) for the clusters in the present sample, ordered by increasing right ascension  $\alpha$ . Equatorial coordinates refer to the J2000.0 equinox.

Cluster name	$\alpha_{2000}$ hh:mm:ss	$\delta_{2000}$ dd:mm:ss	$l$ °	$b$ °
vdBH 73	09:31:56	-50:13:00	273.634	0.951
RUP 85	10:01:33	-55:01:12	280.150	0.160
vdBH 85	10:01:52	-49:34:00	276.914	4.544
vdBH 87	10:04:18	-55:26:00	280.719	0.059
TR 12	10:06:29	-60:18:00	283.828	-3.698
RUP 87	10:15:32	-50:43:00	279.372	4.883
vdBH91	10:17:16	-58:42:00	284.030	-1.600
RUP 88	10:18:55	-63:08:00	286.661	-5.186
vdHB92	10:19:07	-56:25:00	282.984	0.438
TR 13	10:23:48	-60:08:00	285.515	-2.353
vdBH 106	10:52:42	-54:14:00	286.048	4.700
RUP 162	10:52:54	-62:19:00	289.638	-2.545
Lynga 15	11:42:24	-62:29:00	295.053	-0.672
Loden 565	12:08:06	-60:43:12	297.650	1.710
NGC 4230	12:17:20	-55:06:06	298.025	7.445
NGC 4349	12:24:08	-61:52:18	299.719	0.830

**Table 1.** List of objects surveyed in the present article. Note: *For the sake of saving space we indicate van den Bergh-Hagen clusters using the vdBH abbreviations all along the text. In a similar way Ruprecht and Trumpler clusters are mentioned as RUP and TR followed by the respective numbers.*

Positions of the clusters in the Galaxy are shown in Fig. 1 superposed onto the Aladin Sky Atlas DSS2 color image. Our sampling chiefly covers the region around Carina OB association and the south-east part of Vela with some objects in Crux and Centaurus.

## 3. Photometric observations

A first series of CCD *UBVI* photometry was carried out in 13 open clusters placed in the galactic region going from 280° to 300° in galactic longitude and from 7° to -5° in galactic latitude. This region covers the Carina Arm, the inter-arm region

between the Perseus and Carina arms and also a part of the Local Arm. Observations were made using the YALO facilities at Cerro Tololo Inter-american Observatory on 9 nights in April and May 2002. Images were taken with a 2048 × 2048 Tek CCD attached to the 90-cm telescope and the standard set of *UBVI* filters available at CTIO. The 0.39 arcsec/px plate scale resulted in a field of view of 13 × 13 arcmins. Images were acquired using the CTIO ARCON operating in Quad mode<sup>1</sup>. The CCD gain was set at 3.2 e<sup>-</sup>/adu and the readout noise was determined to be 4.0 e<sup>-</sup>.

A second series of CCD photometry was implemented during 2 nights (February and March 2010) at Cerro Tololo Inter-american Observatory to get *UBVI* photometry in two other clusters, NGC 4349 and Lynga 15, at a slightly larger galactic longitude (298°). Images in a first run were taken with the CTIO 0.9 m telescope using a 2048 × 2046 px detector with a scale 0.401"/px covering thus 13.6 arcmin on a side. A second run of images taken at the 1.0 m telescope of the same clusters was carried out with a 4064 × 4064 px CCD with a scale of 0.289 arcsec/px thus covering 20' × 20' on a side. The first run (at the 0.9 m) was not photometric, and therefore we tied all the images to the second night (at the 1.0 m), which was photometric. During this second night, we took multiple images of the standard star fields PG 1047 and SA98 (Landolt 1992), covering an air mass range 1.15 – 2.2.

Details of exposure times per filter and telescope can be seen in Tables 2 and 3 for the first and second series respectively.

Short exposures were always obtained to avoid bright star saturation in the frame. Notwithstanding, sometimes we could not help to lose very bright stars. Finally, in the years of 2014 and 2015 the open cluster vdBH 73, located at a smaller longitude (approx. 273°) was observed in the *UBVI* filters with the 1 m Swope telescope at Las Campanas Observatory, Chile. On this occasion, direct images were acquired with the 4kx4k-4 CCD. All observations were made under air mass ranges from 1.08 to 1.092 for *U*, 1.072 for *B* and 1.077 to 1.164 for *V* and *I*.

### 3.1. Photometric reduction process

The basic reduction of the CCD science frames has been done in the standard way using the IRAF 4 package *ccdred*. The photometry was performed using IRAF's DAOPHOT (Stetson 1987; Stetson et al. 1990) and *photcal* packages. Aperture photometry was performed to obtain the instrumental magnitudes of standard stars and some bright cluster stars. Profile-fitting photometry was performed in each program frame by constructing the corresponding point spread function. The zero-point of the instrumental magnitudes for each image was determined with small-aperture photometry and growth curves.

The transformation equations to convert instrumental magnitudes into the standard system were always of the form:

$$\begin{aligned}
 u &= U + u_1 + u_2 X + u_3 (U - B) \\
 b &= B + b_1 + b_2 X + b_3 (B - V) \\
 v &= V + v_1 + v_2 X + v_3 (B - V) \\
 i &= I + i_1 + i_2 X + i_3 (V - I)
 \end{aligned}$$

where  $u_2, b_2, v_2, i_2$  are the extinction coefficients computed for each night and  $X$  is the air-mass. In each case detector

<sup>1</sup> <http://www.ctio.noao.edu/instruments/arcon/arcon.html>

../figs/DSS2color.png

**Fig. 1.** DSS2 color Aladin image showing with white circles the position of the clusters surveyed in the present sample. The galactic coordinates  $l$  and  $b$  are depicted by a green grid while constellation limits for Carina, Vela, Centaurus and Crux appear in yellow lines.

Cluster	Date	Pass band				
		U	B	V	R	I
Exp. Times (secs)		long/short	long/short	long/short	long/short	long/short
RUP 85	04/04/2002	300/30	200/5	160/3	160/2	120/1
vdBH 85	04/05/2002	300/30	200/5	160/3	160/2	120/1
vdBH 87	04/06/2002	300/30	200/5	160/3	160/2	120/1
TR 12	04/09/2002	300/30	200/5	160/3	160/2	120/1
RUP 87	04/19/2002	300/30	200/5	160/3	160/2	120/1
vdBH 91	05/02/2002	300/60	200/20	160/10	160/10	120/10
RUP 88	05/03/2002	300/60	200/20	160/10	160/10	120/10
vdBH 92	05/07/2002	300/60	200/20	160/10	160/10	120/10
vdBH 106	05/07/2002	300/60	200/20	160/10	160/10	120/10
Loden 595	05/08/2002	300/60	200/20	160/10	160/10	120/10
RUP 162	05/08/2002	300/60	200/20	160/10	160/10	120/10
TR 13	05/08/2002	300/60	200/20	160/10	160/10	120/10

**Table 2.** Log of observations at YALO.

Date	U	B	V	I
CTIO 1m				
03/11/2010	30/200	20/150	20/100	20/100
CTIO 0.9m				
02/13/2010	5/2400	3/1800	3/1100	3/1100
Swope				
04/30/2011			15/900	
04/30/2014		30/1500		
05/01/2014	60/2000			
06/13/2015				15/450

**Table 3.** Log of observations at CTIO and Las Campanas

coordinates were cross-matched with 2MASS (Skrutskie et al. 2006) to convert pixels into equatorial  $\alpha$  and  $\delta$  for equinox J2000.0, thus providing 2MASS-based astrometry for the entire catalog.

With the exception of the cluster NGC 4349, the rest of the objects in our sample have no optical photometric studies so that no comparison with previous photometry is possible. Notwithstanding we could perform a comparison of our photometry in  $V$  and  $(B - V)$  with available photometry from APASS (The AAVSO Photometric All-Sky Survey<sup>2</sup>). In this comparison we have put special care in those clusters belonging to the observing runs in 2002 since they are for the most part very faint. Therefore we performed a by-eye selection of well isolated stars to avoid light contamination from nearby stars in APASS photometry. In each science frame we have found between 12 and 21 stars in common with APASS, well distributed in magnitude and colors. In the particular case of van den Bergh-Hagen 73 we stated a comparison with APASS data including a larger sample of stars in common (about 300 stars) and the final results for  $V$  and  $(B - V)$  comparisons were of the same order.

<sup>2</sup> <https://www.aavso.org/apass>

Table 4 shows the mean  $\Delta V$  and  $\Delta(B - V)$  results for individual regions. Indeed differences in  $V$  magnitudes were found within reasonable values when comparing both sets of photometry. As for the differences in the  $(B - V)$  color index we found an even better agreement. This fact makes us confident with the closeness of our photometry to the standard photometric system. Final tables containing star number, x,y detector coordinates and alpha, delta absolute coordinates together with magnitude and colors will be published in separate form.

Cluster name	$\Delta V$	$\Delta(B - V)$	N
vdBH 73	$-0.07 \pm 0.06$	$0.00 \pm 0.04$	264
RUP 85	$0.05 \pm 0.09$	$0.00 \pm 0.06$	21
vdBH 85	$-0.01 \pm 0.03$	$-0.08 \pm 0.04$	18
vdBH 87	$-0.00 \pm 0.03$	$-0.01 \pm 0.04$	15
TR 12	$0.03 \pm 0.04$	$-0.05 \pm 0.06$	16
RUP 87	$0.00 \pm 0.03$	$0.00 \pm 0.03$	13
vdBH 91	$0.02 \pm 0.04$	$0.00 \pm 0.03$	15
RUP 88	$0.05 \pm 0.04$	$0.00 \pm 0.03$	18
vdBH 92	$0.04 \pm 0.04$	$-0.02 \pm 0.03$	15
TR 13	$-0.05 \pm 0.03$	$-0.04 \pm 0.01$	14
vdBH 106	$0.04 \pm 0.04$	$-0.03 \pm 0.03$	20
RUP 162	$0.02 \pm 0.07$	$-0.05 \pm 0.07$	14
Lynga15	$0.08 \pm 0.02$	$-0.00 \pm 0.03$	12
Loden 565	$0.03 \pm 0.03$	$-0.06 \pm 0.04$	13
NGC 4230	$0.02 \pm 0.05$	$-0.03 \pm 0.03$	16
NGC 4349	$0.07 \pm 0.04$	$-0.00 \pm 0.04$	19

**Table 4.** Mean differences with APASS

Figure 2 shows the CCD  $V$  images of the clusters areas where we have carried out the photometric surveys. The series of panels shown from upper left to the lower right are ordered by increasing right ascension and labeled with the cluster name inserted in every panel. Absolute decimal coordinates,  $\alpha$  and  $\delta$ , for the J2000.0 equinox are shown in each panel as reference for the reader. Coordinates should not be read from images.

Final tables containing star numbering and final photometry for each cluster can be found at [\(Insert link for table\)](#).

#### 4. Photometric data analysis process: Gaia data and the ASteCA code

Given the large number of objects observed in this paper and regarding a systematic, reproducible and homogeneous analysis the ASteCA code<sup>3</sup> is the optimal tool to process our set of clusters. The main goal of this code is to put the user apart, as much as possible, from the analysis of a stellar cluster to derive its fundamental parameters. We shall limit ourselves to give a brief summary about the way the positional and photometric data are employed by the code. A complete description of the analysis carried out by ASteCA can be found in Perren et al. (2015) and Perren et al. (2017).

##### 4.1. Gaia data

The second data release for the Gaia mission (Gaia Collaboration et al. 2018) was presented on April 2018 with improved coverage, particularly for the five-parameter astrometric solution. We crossed-match our complete set of photometric data with those

of Gaia DR2 and employed Gaia’s  $G$  magnitude, parallax, and proper motions in our analysis as described in Sect4.2.

No “a priori” cut-off has been done on Gaia DR2 parallax or proper motion data following the advice given in Luri et al. (2018). The parallax values were processed with a Bayesian approach to derive an independent estimate of the distance to each cluster. In this approach, the model for the cluster is taken from the accompanying tutorial by Bailer-Jones on inferring the distance to a cluster via astrometry data<sup>4</sup>. Our model marginalizes not only over the individual distances but also over the shape parameter, estimating only the overall cluster distance using the parallax value and its uncertainty for each star in the decontaminated cluster region (cleaned from contaminating field stars through the membership probabilities process described in Sect. 4.2). The prior for the Bayesian model is a Gaussian centered at a maximum likelihood estimate of the distance to the cluster region, with a large standard deviation of 1 Kpc and a cut-off for negative values. The results of this analysis will be shown in a  $Plx$  vs  $G$  plot for each cluster in Sect 5. We also performed the naive estimate of obtaining the median of stars with parallax values greater than zero and the weighted average values (where the weights are the inverse of the parallax errors). In general, the Bayesian distance estimates are larger than the photometric distances obtained with ASteCA. We followed the advice given in Lindegren et al. (2018) and added 0.029 mas to the parallax values, since there is an offset in the zero point from Gaia DR2. Even after applying this offset, the distance estimates obtained from the Bayesian method and the parallax values are consistently larger than the photometric distances. The match improves applying instead the 0.054 mas and 0.075 mas offsets by Schönrich et al. (2019) and Xu et al. (2019) respectively. This points to a potential local systematic quantity larger than  $\sim 0.05$  mas found affecting Gaia DR2 parallaxes.

We also include a two-sample Anderson-Darling test,<sup>5</sup> comparing the distribution of Gaia DR2 data (parallax and proper motions) between the cluster and the estimated stellar field regions, to quantify how “similar” these two regions are among each other. We report the results of the test in each case indicated with AD, together with their corresponding p-value<sup>6</sup>. The p-value indicates at what significance level the null hypothesis can be rejected, where a small p-value means that we can safely reject the null hypothesis. Smaller p-values thus imply that the samples (cluster region vs field region) do not come from the same distribution, which means a larger probability for the cluster region of being a true physical entity rather than a random clustering of field stars. Since we use the parallax data and each proper motion dimension to obtain the Anderson-Darling test, this results in three different p-values for each cluster. These are combined into a single p-value using Fisher’s combined probability test<sup>7</sup>.

<sup>4</sup> <https://github.com/agabrown/astrometry-inferencetutorials>

<sup>5</sup> [https://docs.scipy.org/doc/scipy/reference/generated/scipy.stats.anderson\\_ksamp.html](https://docs.scipy.org/doc/scipy/reference/generated/scipy.stats.anderson_ksamp.html)

<sup>6</sup> The null hypothesis ( $H_0$ ) is the hypothesis that the distributions of the two samples are drawn from the same population. The significance level ( $\alpha$ ) is the probability of mistakenly rejecting the null hypothesis when it is true, also known as Type I error. The p-value indicates the  $\alpha$  with which we can reject  $H_0$ . The usual 5% significance level corresponds to an AD test value of 1.961, for the case of two samples.

<sup>7</sup> [https://docs.scipy.org/doc/scipy/reference/generated/scipy.stats.combine\\_pvalues.html](https://docs.scipy.org/doc/scipy/reference/generated/scipy.stats.combine_pvalues.html)

<sup>3</sup> <http://asteca.github.io/>

By way of example, one of the clusters with the largest combined p-value (0.216) is vdB-Hagen 91, which means that it is the region less likely to contain a real star cluster (according to this statistical test based on parallax and proper motion data).

#### 4.2. The way ASteCA works

The several tasks performed by ASteCA can be roughly divided into three main analysis blocks: structural study including the determination of a cluster region identified primarily by an overdensity, individual membership probability estimation for stars inside the overdensity, and the search for the best fit parameters.

The first block is in charge of estimating the center and radius values that define the cluster region. We know that robust estimations of these two quantities can only be achieved when a clear overdensity and a large number of members are detected. In the case of clusters that are not clearly defined as an overdensity on the observed frame and whose boundary is weakly established, ASteCA allows center and radius to be manually fixed since the automatic procedure may return incorrect values. The group of clusters in this work is structurally sparse and, “a priori”, with a low number of members. In many cases, therefore, central coordinates and radius value that determine the cluster region have been set manually. King profiles fitting have been performed for those cases when a fit could be generated. No formal core or tidal radius are given because their values, due mainly to the shape of the radial density profile (hereafter RDP), were not within reasonable estimates.

Every point of the RDP is obtained by generating “square rings” around the center defined for the potential cluster, i.e.: the comparison field. In the present case the comparison field may contain between 1 and 10 regions of equal area to that of the cluster, depending on the cluster area and the available size of the remaining of the frame. In each ring the found number of stars is divided by the respective area to get a value of the radial density. For the computation of the density level of the field (foreground/background), outliers in the RDP are iteratively discarded to avoid biasing the final value. This procedure is repeated until converging to an equilibrium value, equivalent to the density of the star field at a given distance from the potential cluster center.

The second analysis block assigns membership probabilities, a process that is usually disregarded in simpler cluster studies. By itself, an overdensity does not imply the existence of a real cluster since many times it may also come from random fluctuations in the field star density. To discard this possibility a rigorous comparison of the photometric properties for cluster and field stars must be done. Eventually, what we are looking for is firm evidence of the presence of a cluster sequence at some evolutionary status. This is accomplished by employing a Bayesian algorithm that compares the photometric, parallax, and proper motions distribution of stars in the cluster region, with the distribution of stars in surrounding field areas (Perren et al. 2015). In the present case, this implies the analysis of a 7-dimensional data space ( $G$  magnitude;  $(V - I)$ ,  $(B - V)$ ,  $(U - B)$  colors; parallax; and proper motions). Briefly, the algorithm compares the D-dimensional data associated to stars within the adopted cluster limits, to the data associated to stars in regions of equivalent area outside the cluster. The position of every star inside the cluster in this data space is compared against each star in all the defined equivalent-area field regions, assuming a Gaussian probability

density (centered at the given values for each data dimension, with standard deviations given by the respective uncertainties). This procedure is repeated hundreds or thousands of times (defined by the user) each time selecting different stars to construct an approximation of the clean cluster region. The outcoming result of this algorithm are thousands of probability values that are averaged to a final and single membership probability value for each star within the cluster region.

A next step in this process consists in the cleaning of the photometric diagrams for the cluster region. Now, each photometric diagram for the adopted cluster area is divided into cells and similarly for the equivalent diagram of the field. The density number found in the field is then subtracted from the cluster photometric diagram, cell by cell, starting with stars having low membership probabilities. Therefore, the final cluster photometric diagrams contain not only star membership assignment but it is also cleaned from the expected field star contamination. This two-step process is of the utmost importance to ensure that the fundamental parameters analysis is performed on the best possible approximation to the cluster sequence (particularly when the cluster contains few members).

Finally, the third block performs the cluster’s parameters estimation through the minimization of a likelihood function (Dolphin 2002) employing a genetic algorithm numerical optimization (Charbonneau 1995). This last stage includes the assignment of uncertainties for each fitted parameter via a standard bootstrap method (Efron & Tibshirani 1986). Again, all of these processes are described in much more detail in Perren et al. (2015) and Perren et al. (2017).

It is worth noting that, unlike other tools (e.g.: Yen et al. 2018), ASteCA does not fit isochrones to cluster sequences in photometric diagrams. Although the use of this method is widespread for its simplicity, it is merely a geometrical fitting which does not include the full physics of the problem. Instead, ASteCA fits two or three-dimensional synthetic clusters in color-magnitude diagrams (depending on the number of photometric colors available) generated from a set of theoretical isochrones, a given initial mass function, and completeness and uncertainties functions estimated directly from the observations. The “best fit” isochrones shown in green in the respective photometric diagrams are there for convenience purposes only, as a way to guide the eye.

The processing of these sixteen stellar clusters with ASteCA makes use of the PARSEC v1.2S (Bressan et al. 2012) theoretical isochrones (obtained from the CMD service<sup>8</sup>), and the Kroupa (2002) form for the initial mass function. The full processing results in estimates for the five parameters: metallicity, age, extinction, distance, and mass, along with their respective uncertainties. The binary fraction was fixed to 0.3 for all cases, which is regarded as a reasonable estimate for open clusters (Sollima et al. 2010). The final mass value, although corrected by effects of star loss such as the maximum magnitude observed, does not take into account the dynamical mass loss due to the cluster’s orbiting through the Galaxy. Hence, it should be regarded as the present day mass value, and not the total initial mass value.

In this instance ASteCA proceeds as follows. In a first step, the three dimensional  $G$  vs  $(B - V)$  vs  $(U - B)$  photometric diagram was analyzed with the metallicity fixed to solar value ( $z = 0.0152$ ). This is an acceptable estimate used to reduce the dimensionality of the parameter space, and thus its complexity. Although the aforementioned diagram contains in the present

<sup>8</sup> <http://stev.oapd.inaf.it/cgi-bin/cmd>

case a rather small number of stars due to the presence of the  $U$  filter, it is extremely useful for constructing the  $(U - B)$  vs  $(B - V)$  diagram which is known to be good estimator of reddening and thus of extinction (Vázquez et al. 2008). In all cases, the  $E_{(B-V)}$  estimates were checked against the maximum values given by the Schlafly & Finkbeiner (2011) maps<sup>9</sup>. Thus, the only information extracted from this first step and in particular by inspection of the  $(U - B)$  vs  $(B - V)$  diagram is a reasonable range for the  $E_{(B-V)}$  parameter. In a second step the analysis of the  $G$  vs  $(B - V)$  vs  $(V - I)$  diagram is carried out restricting now the reddening space to the range obtained in the previous step, while still fixing the metallicity to solar value. We obtain from this process estimates for the age, distance, and cluster mass. Finally, a third step uses the ranges derived by the two processes above for the age, extinction, distance, and mass, and adds the metallicity as a free parameter. As a result of the entire process, we obtain a five parameter best model fit for each observed cluster, along with the associated one sigma uncertainties for each parameter. In all the cases we have adopted  $R = A_V/E_{(B-V)} = 3.1$  to produce corrected distance moduli.

After all the processing is done, each observed cluster was finally compared to approximately  $\sim 2 \times 10^7$  synthetic clusters.

## 5. Cluster-by-cluster discussion on structural and intrinsic parameters provided by ASteCA

We show next the results provided by the spatial and photometric analysis carried out with ASteCA, together with the outcome of the application of the Anderson-Darling test that compares parallax and proper motion distributions in the cluster regions and its respective field regions. It is important to emphasize that the ASteCA code will always fit the best possible synthetic cluster to a given star distribution, no matter if we face a true open cluster or not.

Observation and analysis results for each cluster are depicted with four figures. The first of them shows the photometric diagrams built with all the stars observed in the region where a cluster is supposed to exist, according to the literature. The second figure represents the spatial analysis carried out by ASteCA. This is: results from the search of an stellar overdensity, the mean value for the stellar field, the respective King profile<sup>10</sup> attempting to fit the radial density profile, and the assumed radius. The third figure introduces the “clean” color-color  $(U - B)$  vs  $(B - V)$  and the field decontaminated color-magnitude diagrams,  $G$  vs  $(B - V)$  and  $G$  vs  $(V - I)$  (from now on CCD and CMDs respectively), made with stars having membership probabilities provided by ASteCA. We insert in the mid panel of this last figure, the color-color diagram, the results from the best synthetic cluster fitting to the field decontaminated diagrams. In these three panels we show as well the isochrone curves from which the best synthetic cluster fit was generated. Again, this is just to guide the eye since ASteCA does not fit isochrones. The fourth figure, finally, includes three panels. The left one shows the  $G$  mag vs parallax values (uncertainties indicated by horizontal bars) of cluster members, colored according to the membership probabilities estimated by ASteCA (colorbar to the right). These are the stars that are selected by the code after the membership assignment and CMD cleaning processes. The

Bayesian distance found by the code is shown by a vertical blue dashed line, the equivalent ASteCA distance with a green dotted line, the weighted average with a red dashed line and the naive estimate of obtaining the median of stars with parallax values greater than zero with black dashed line. The mid panel in this fourth figure is the kernel density estimate (KDE) of stars in the surrounding field region and the cluster region, in black and red lines respectively. For the Anderson-Darling test we used all the stars within the cluster region with Gaia DR2 data. In the right panel we summarize the distances in parsecs and errors according to the Bayesian analysis ( $d_{Bayes}$ ) and ASteCA ( $d_{ASteCA}$ ) followed by the parallax corresponding value,  $Plx$ , and corrected distance modulus,  $\mu_0$ . Both fittings are indicated by the vertical blue and green dashed lines. The final four text lines in the right panel are the AD values for  $Plx$ ,  $PM(\alpha)$ ,  $PM(\delta)$  from the Anderson-Darling test, followed by the corresponding  $p$ -values and finally the combined  $p$ -value.

Our sample contains clusters with a large variety of properties: some are robust, bright, well detached from the cluster background and therefore with a clearly defined main sequence, others are clusters which are faint, with sparse star population and easy to confuse with the background. Therefore, given the anomalous amount of figures to be shown in this paper we decided to add them to an electronic Appendix to save space, and limited ourselves here to present the case of two extreme types of cluster according to the statement above: a poorly defined (vdBH 73), a well-defined (NGC 4349) and a not cluster (RUP 87).

### 5.1. van den Bergh-Hagen 73

The cluster vdBH 73 is placed in almost the center of the Vela constellation well at the northeast border of the Carina Constellation. The visual chart of the region in Fig. 2 shows a small and compact grouping of stars at the very center of the frame surrounded by a dense stellar field. However, the inspection of the CCD and CMDs for all the observed stars in Fig. 3 gives no hints about the presence of a cluster there. Basically, there are in the CMDs of Fig. 3 few stars above  $V = 15$  mag but at larger magnitudes the CMDs strongly widen surely due to the presence of increasing visual absorption. In fact, the reddening in the CCD, right panel in Fig. 3, is quite strong and displaces the bulk of stars entirely toward the red side. Even some blue stars with negative  $(U - B)$  values appear strongly affected by variable reddening.

The ASteCA spatial data processing shows a pronounced star overdensity of 2.5 arcmin radius in the left panel in Fig. 4 coincident with the location expected for vdBH 73. This overdensity appears very well detached from the field star mean density as seen in the RDP to the right. Notice that the density peak is about five times above the mean for the field.

In the following step the removal of field interlopers by comparison with the background field properties yielded the clean diagrams for all stars with membership probability above 0.46 which are shown in Fig. 5. The clean CMDs, left and right panels, put in evidence a cluster main sequence subtending 1.5 magnitudes and a faint giant branch with stars up to  $V = 15$  mag. The clean CCD in the middle panel shows only a handful of stars with no clear locus defined. All these stars have membership probabilities between 0.46 and 0.93 favoring thus the true nature of this object. This is: such a level of probability suggests that stars in the adopted cluster region are –for the most part– well detached,

<sup>9</sup> Through the NASA/IPAC service <https://irsa.ipac.caltech.edu/applications/DUST/>

<sup>10</sup> We recall that in the present investigation given the small number of members in each cluster and the particular geometry of these objects, the King profile fitting is of no relevance.

in terms of their photometric characteristics and spatial distribution, from those belonging to the cluster surroundings and therefore with low chance to be confused with the stellar field. The best fitting of a synthetic cluster yields the following facts:

- a) The cluster is immersed in a region of moderate absorption since the mean of reddening comes to be  $E_{(B-V)} = 0.62$ , a value compatible with the ones provided by Schlafly & Finkbeiner (2011) (hereafter S&F2011) who found a maximum  $E_{(B-V)}$  of about 1.2 mag towards vdBH 73.
- b) The absorption-free distance modulus turns out to be 12.1 placing this object at 2.6 kpc from the Sun.

From the photometric point of view the existence of a well outlined cluster main sequence and the high probability memberships of the stars seen in it confirm the real entity of vdBH 73. However, the usage of parallax data from Gaia, see Fig. 6, shows a huge difference in distance reaching up 2.7 kpc in the sense that Gaia DR2 parallaxes place the cluster farther than photometry does. This difference improves when offset is applied to the parallax data, as shown in Sect. 7. The Anderson-Darling test applied to parallax and proper motion data demonstrates that the null hypothesis can indeed be rejected, pointing to a real cluster present in this region.

We conclude from our analysis that van den Bergh 73 is an old cluster around  $6 \times 10^9$  years old.

## 5.2. NGC 4349

This is a Crux constellation object, placed slightly south of the Crux geometric center. At first glance, the  $V$  image in Fig. 2 shows a distinguishable star accumulation. The overall photometric CCD and CMDs in Fig. 7 show a prominent star sequence emerging at  $V = 16$  mag from the usual stellar structure produced by disc stars. The CCD makes more evident the presence of a reddened but compact sequence of blue stars placed immediately below the first knee of the intrinsic line. Apart from this, other bluer stars appear for  $(U - B)$  values smaller than 0.0.

ASteCA analysis revealed an extended overdensity of up to 20 stars per square arcmin reflected by a prominent but a tiny RDP with a radius of 4.5 arcmin depicted in the panels of Fig. 8. The ASteCA estimation of memberships shows that inside the adopted cluster radius the probability values go from 0.41 to 1.0 in the respective CCD and CMDs of Fig. 9. So, it is clear that probable members of the cluster detach easily from the field region stars photometric properties. If attention is drawn to the largest probabilities (say above 0.7, starting in light blue symbols) there appears in the three diagrams a somewhat narrow cluster. Comparison with synthetic clusters yielded that NGC 4349 is a cluster with the following properties:

- a) A color excess of  $E_{(B-V)} = 0.40$  is found for the best fitting synthetic cluster. Since the maximum color excess provided by S&F2011 in this location is 2.83 one concludes that most of the absorption is produced behind the position of NGC 4349.
- b) The absorption free distance modulus of NGC 4349 is 12.2, placing it at a distance of  $d = 2.75$  kpc from the Sun.

NGC 4349 is the only cluster in our sample with previous photographic photometry in the  $UBV$  system performed by

Lohmann (1961). Given the usual large differences between photographic and CCD photometry we performed no comparison between the Lohmann data-set and ours. According to Lohmann (1961), NGC 4349 is located at a distance of  $d = 1.7$  kpc, far enough from our estimate. However, coincidences in terms of reddening, size and background star density have been found since Lohmann stated a cluster reddening of  $E_{(B-V)} = 0.38$  and similar cluster size. On the other hand, the Kharchenko Atlas<sup>11</sup> (Kharchenko et al. 2005) gives a reddening value of  $E_{(B-V)} = 0.38$  quite similar to ours although the distance reported,  $d = 2.1$  kpc, is slightly below our estimate. It is worth noting that the distance found for this cluster using Gaia DR2 parallax data with no applied offset, processed with the Bayesian method described in Sect. 4.1, is lower than the photometric distance found by ASteCA, 2.23 kpc, and gets lower as larger offsets are applied.

Parallax and proper motion distributions were tested using the Anderson-Darling statistics. With the exception of the comparison in the case of  $PM(\delta)$  (where both samples, cluster and field, seem to come from the same distribution at a critical value just above 5%) the remaining two tests report quite different samples confirming, together with the photometric results, the true nature of NGC 4349.

High probability values for stars inside the overdensity confirm the true nature of this object since the over density and the density profile are followed by a very well defined and extended photometric counterpart. Since all these facts are self-consistent, we are confident that NGC 4349 is an open cluster around  $396 \times 10^6$  years old. The Kharchenko Atlas gives quite a similar value for the cluster age, reporting  $\log(t) = 8.32$  equivalent to  $209 \times 10^6$  yrs.

## 5.3. Ruprecht 87

RUP 87 is in the east side of the Vela constellation. According to the respective Fig. 2 there is no relevant feature but a rather poor and boring stellar field. The first glance impression is confirmed in the photometric diagrams since no appreciable stellar structure defining the presence of an open cluster is present in the overall CMDs of Fig. 11. The few stars with  $(U - B)$  measures plotted in the respective color-color magnitude resemble a typical CCD of a galactic field dominated by a handful of late  $F$  and  $G$ -type stars followed by a pronounced tail of red stars presumably of evolved types. Perhaps stars in the region  $0 < (U - B) < 0.5$  and  $0 < (B - V) < 0.6$  are reddened early  $A$  or/and late  $B$ -types.

Accordingly, after many essays ASteCA could not define the presence of an overdensity as obviously seen in Fig. 12. The inability of our code to identify any overdensity simply means that the potential locus occupied by the cluster RUP 87 is not unambiguously separated from the field background stars. So, after many attempts to state the place of the cluster we decide to focus the attention in the region encircled by a green line. However, the RDP emerging from this analysis is not only quite noisy but it is hard to establish the mean value of the background density. Notice that only 28 stars remain in the region adopted. The estimation of the memberships and the not so clear clean CCD and CMDs in Fig. 13 reflects the difficulty since stars inside the adopted cluster area have membership values ranging from 0.34 to 0.81 so that a significant portion of those may also

<sup>11</sup> <https://webda.physics.muni.cz/cocd.html>



belong to the surrounding field.

As seen in Fig. 14 the Anderson-Darling test values for  $Plx$  and proper motions do not confirm clear differences between the cluster region and the stellar background in terms of kinematics and distance. The poverty of the photometric diagrams and the analysis of Gaia data are all against the true existence of a cluster in the region RUP 87. In our interpretation this is not a real entity but a fluctuation of the star field.

## 6. Gaia parallax distances analysis

In an ulterior step we draw the attention to Gaia DR2 parallax data to perform a fast computation of distances and compare them with the findings from the analysis of the photometry. In this context  $Plx$  data were cross-matched with our photometry and processed within a Bayesian framework. As seen in the last two columns of Table 5 distances from ASteCA are almost always smaller than the ones coming from our computation of parallax values provided by Gaia DR2. The exceptions are NGC 4349, and vdBH 106 which show smaller photometric distances (particularly vdBH 106). The situation is more clearly shown in Fig. 15 (top) with a plot of ASteCA distances against those obtained from Gaia DR2 parallaxes, with no bias applied.

If we add the offsets (0.029, 0.054, 0.075) mas to the parallax data following the results presented in Lindegren et al. (2018), Schönrich et al. (2019), and Xu et al. (2019) respectively, we see that the agreement between photometric and Gaia DR2 distances improves as shown in Fig. 16. The general mean differences between photometric distances (estimated with ASteCA) and parallax distances (Gaia DR2 parallax data corrected by a bias value and processed with a Bayesian method) are of  $\sim -347$  pc,  $\sim -33$  pc, and  $\sim 208$  pc, using the bias corrections from Lindegren et al., Schönrich et al., and Xu et al. respectively. This tends to confirm that a larger bias correction for the parallax is needed than that proposed by Lindegren et al. Two clusters show no good agreement between photometric and parallax distances with either bias correction: vdBH 73, and van den Bergh-Hagen 106. vdBH 73 is well defined but faint while vdBH 106 shows a very dispersed sequence in its CMD. If we repeat this estimations leaving out these two clusters, the above values change to  $\sim -398$  pc,  $\sim -92$  pc, and  $\sim 114$  pc, again for Lindegren et al., Schönrich et al., and Xu et al. respectively. This analysis points to a required bias correction to Gaia DR2 parallax data between those of Schönrich and Xu. If we look at Fig 15 (bottom) we will see that the offset found when comparing with parallax distances obtained with no bias applied, is around  $\sim 0.07$  mas. The offset value found in this study is thus closest to the Xu et al. bias estimation.

There are additional reasons to be taken into account in terms of disagreements between Gaia distances and those obtained photometrically. On one hand, ASteCA does not fit for the value of  $R$  (ratio between visual absorption and excess color, fixed at  $R = 3.1$ ) and it is known that variations in  $R$  can modify distances and ages. However, these differences in distances are very appreciable only among young clusters, but not among the older ones. ASteCA also has some degree of difficulty in estimating the parameters of young clusters because their main sequences are appreciably vertical and this can introduce an appreciable fit uncertainty when there are also few members. This could explain the great difference with the Gaia distance that exists in the case of RUP 162 (added to the fact that this one, in particular, may not be a real cluster). But on the other hand, ASteCA fits more precisely those clusters where there is a well defined main se-

quence followed by a not ambiguous turn-off point such as the case of vdBH 85. And yet the differences between photometric distances and Gaia for this object is among the largest, when no offset is applied.

## 7. Discussion of results and concluding remarks

In the precedent sections we have analyzed the fields of sixteen potential open clusters located in a Galaxy sector covering from  $290^\circ$  to  $320^\circ$  approximately in galactic longitude, and the formal galactic plane at  $b = 0^\circ$ . The cluster parameter estimations presented in this article are based on precise  $UBVI$  photometry analyzed in a automatic way by our code ASteCA. The code looks for a meaningful stellar overdensity assigning membership probabilities by comparison with the surrounding stellar field. The next step establishes the physical properties of the best synthetic cluster that fits the distribution of cluster members in the CMDs and the CCD. Through this process reddening, distance, age, mass, and metallicity are given. The most relevant inconvenient we have found with the present cluster sample resides in the fact that they are extremely faint, which becomes evident by visual inspection in the overall CCD and CMD. To make things worse the  $(U - B)$  index has been majorly available for the bright and blue stars which reduced considerably the data analysis space. Despite this we were able to keep the reddening solutions under control and obtain reliable distances estimations. An interesting data provided by ASteCA analysis is the metallicity  $z$  for each cluster included in the third column of Table 5. The average value including all the clusters is  $z = 0.0153$  with a standard deviation  $\sigma = 0.009$  well in agreement with modern adopted values for solar metallicity as expected in most of open clusters.

We can finally discard the following objects from our cluster sample: RUP 87, vdBH91, RUP 88, Lynga 15, Loden 565 and NGC 4230 since they are most probably random stellar fluctuations. The results for true and probable open clusters are shown in Table 5 in self-explicative format.

We can also conclude that by adding  $\sim 0.07$  mas to the cluster computed parallaxes from Gaia DR2 parallax data, the level of agreement with the photometric distances is reasonable. For other objects the gap between photometric and parallax distances narrows when a smaller offset is applied instead, but the decision of adding either quantity becomes somewhat arbitrary. Our cluster sample is not large enough to permit us drawing stronger conclusions on this regard.

Regarding the spiral structure in this portion of the galaxy we cannot add much. Only three clusters are young enough to be considered spiral structure tracers. As seen in Fig. 17, two of them, TR 13 and RUP 162, are located along the Carina arm. In particular, at the distance at which TR 13 is located, it comes to be placed 200 pc below the plane thus accompanying the warp of this arm already mentioned by, among others, Cersosimo et al. (2009) A third cluster, vdBH 162, is located in an intermediate zone between the Sun and Carina's arm. None of the objects in our sample is, therefore, related to the arm of Perseus.

## References

- Aller, L. H., Appenzeller, I., Baschek, B., et al., eds. 1982, Landolt-Börnstein: Numerical Data and Functional Relationships in Science and Technology



<i>Cluster</i>	<i>z</i>	<i>E</i> <sub>(B−V)</sub>	<i>Age</i> (10 <sup>6</sup> yr)	<i>Mass</i> ( <i>M</i> <sub>⊙</sub> )	<i>d</i> <sub>AS<sub>te</sub>CA</sub> (kpc)	<i>d</i> <sub>Bayes</sub> (kpc)
vdBH 73	0.0208±0.0046	0.62±0.04	6067±1150	1000±800	2.64±0.36	5.32±0.43
RUP 85	0.0259±0.0066	1.06±0.04	412±60	2700±650	4.96±0.40	5.30±0.25
vdBH 85	0.0152±0.0024	0.28±0.03	7396±930	2750±300	4.15±0.24	6.15±0.37
vdBH 87	0.0250±0.0043	0.58±0.01	320±160	1000±250	1.80±0.05	2.37±0.07
TR 12*	0.0060±0.0013	0.29±0.03	800±180	720±100	3.03±0.17	3.97±0.14
vdBH 92	0.0065±0.0029	0.66±0.03	83±40	400±75	1.96±0.11	2.48±0.13
TR 13	0.0073±0.0034	0.55±0.01	27±11	500±150	3.99±0.23	5.02±0.18
vdBH 106*	0.0089±0.0041	0.30±0.03	9705±840	1850±350	6.30±0.62	5.06±0.46
RUP 162*	0.0028±0.0015	0.47±0.02	31±11	550±100	2.82±0.16	4.18±0.22
NGC 4349	0.0277±0.0058	0.40±0.03	396±120	1100±250	2.75±0.17	2.29±0.12

**Table 5.** The symbol “\*” indicates probable clusters. The *d*<sub>Bayes</sub> values are those obtained using the Bayesian method and no bias correction applied on the Gaia DR2 parallax data.

- New Series ” Gruppe/Group 6 Astronomy and Astrophysics ” Volume 2  
Schaifers/Voigt: Astronomy and Astrophysics / Astronomie und Astrophysik  
” Stars and Star Clusters / Sterne und Sternhaufen

Avedisova, V. S. 2002, Astronomy Reports, 46, 193

Bossini, D., Vallenari, A., Bragaglia, A., et al. 2019, A&A, 623, A108

Bressan, A., Marigo, P., Girardi, L., et al. 2012, MNRAS, 427, 127

Cantat-Gaudin, T., Jordi, C., Vallenari, A., et al. 2018, A&A, 618, A93

Cersosimo, J. C., Mader, S., Figueroa, N. S., et al. 2009, ApJ, 699, 469

Charbonneau, P. 1995, The Astrophysical Journal Supplement Series, 101, 309

Dolphin, A. E. 2002, Monthly Notices of the Royal Astronomical Society, 332, 91

Efron, B. & Tibshirani, R. 1986, Statist. Sci., 1, 54

Gaia Collaboration, Brown, A. G. A., Vallenari, A., et al. 2018, ArXiv e-prints [arXiv:1804.09365]

Janes, K. & Adler, D. 1982, The Astrophysical Journal Supplement Series, 49, 425

Kharchenko, N. V., Piskunov, A. E., Röser, S., Schilbach, E., & Scholz, R.-D. 2005, A&A, 438, 1163

Kroupa, P. 2002, Science, 295, 82

Landolt, A. U. 1992, AJ, 104, 340

Lindgren, L., Hernández, J., Bombrun, A., et al. 2018, A&A, 616, A2

Lohmann, W. 1961, Astronomische Nachrichten, 286, 105

Luri, X., Brown, A. G. A., Sarro, L. M., et al. 2018, ArXiv e-prints [arXiv:1804.09376]

Magrini, L., Stanghellini, L., Corbelli, E., Galli, D., & Villaver, E. 2009, VizieR Online Data Catalog, J/A+A/512/A63

Moitinho, A. 2010, in IAU Symposium, Vol. 266, Star Clusters: Basic Galactic Building Blocks Throughout Time and Space, ed. R. de Grijs & J. R. D. Lépine, 106–116

Moitinho, A., Vázquez, R. A., Carraro, G., et al. 2006, MNRAS, 368, L77

Perren, G. I., Piatti, A. E., & Vázquez, R. A. 2017, A&A, 602, A89

Perren, G. I., Vázquez, R. A., & Piatti, A. E. 2015, A&A, 576, A6

Schlafly, E. F. & Finkbeiner, D. P. 2011, ApJ, 737, 103

Schönrich, R., McMillan, P., & Eyer, L. 2019, MNRAS, 487, 3568

Skrutskie, M. F., Cutri, R. M., Stiening, R., et al. 2006, AJ, 131, 1163

Sollima, A., Carballo-Bello, J. A., Beccari, G., et al. 2010, MNRAS, 401, 577

Soubiran, C., Cantat-Gaudin, T., Romero-Gómez, M., et al. 2018, A&A, 619, A155

Stetson, P. B. 1987, PASP, 99, 191

Stetson, P. B., Davis, L. E., & Crabtree, D. R. 1990, in Astronomical Society of the Pacific Conference Series, Vol. 8, CCDs in astronomy, ed. G. H. Jacoby, 289–304

Tadross, A. L. 2011, Journal of Korean Astronomical Society, 44, 1

Vázquez, R. A., May, J., Carraro, G., et al. 2008, ApJ, 672, 930

Xu, S., Zhang, B., Reid, M. J., Zheng, X., & Wang, G. 2019, arXiv e-prints, arXiv:1903.04105

Yen, S. X., Reffert, S., Schilbach, E., et al. 2018, ArXiv e-prints [arXiv:1802.04234]

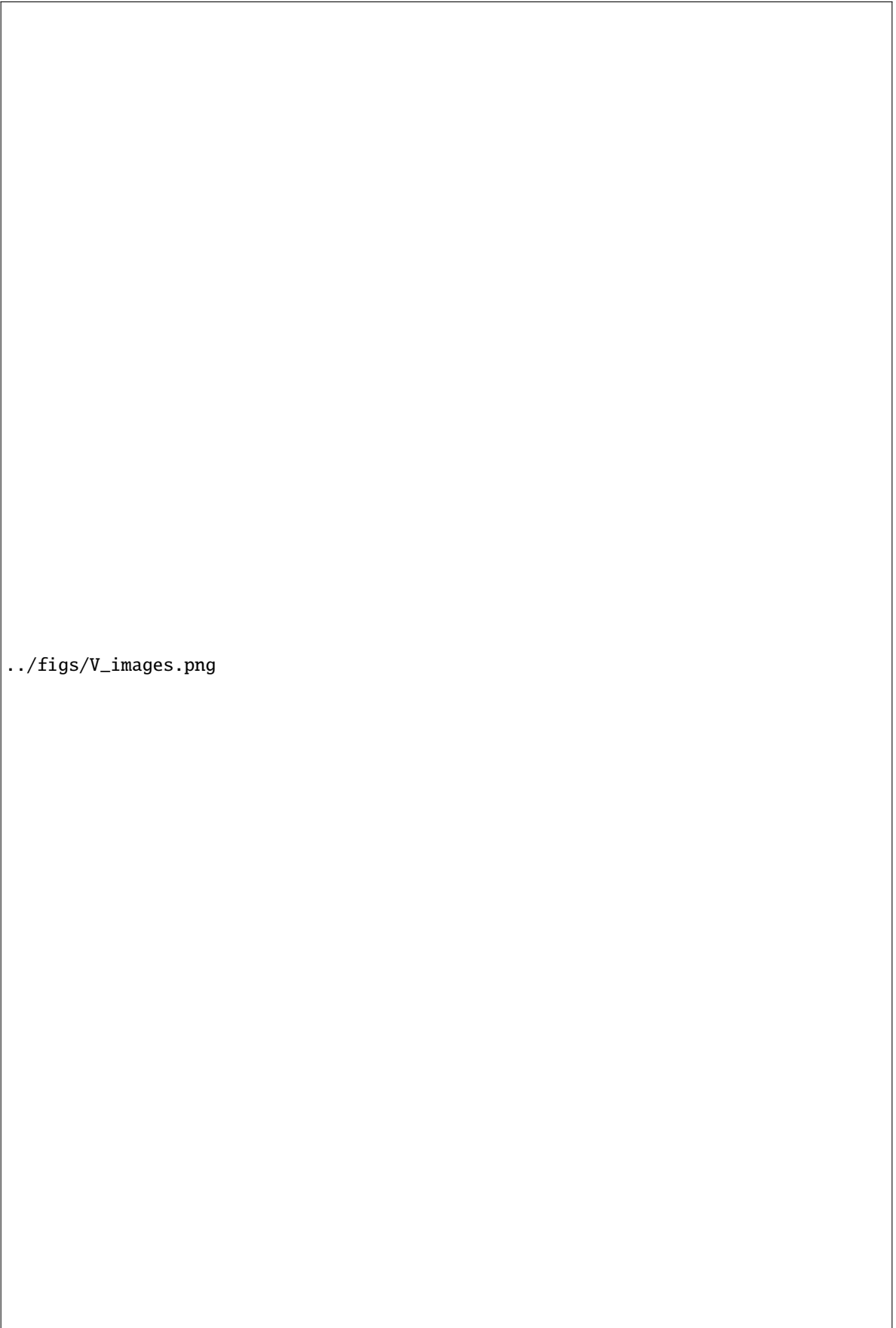


**Fig. 2.** The V images of the observed clusters (names inserted) ordered from top to bottom and from left to right by increasing right ascension. Decimal  $\alpha$  and  $\delta$  coordinates for the 2000 equinox are indicated. North and East are also shown.

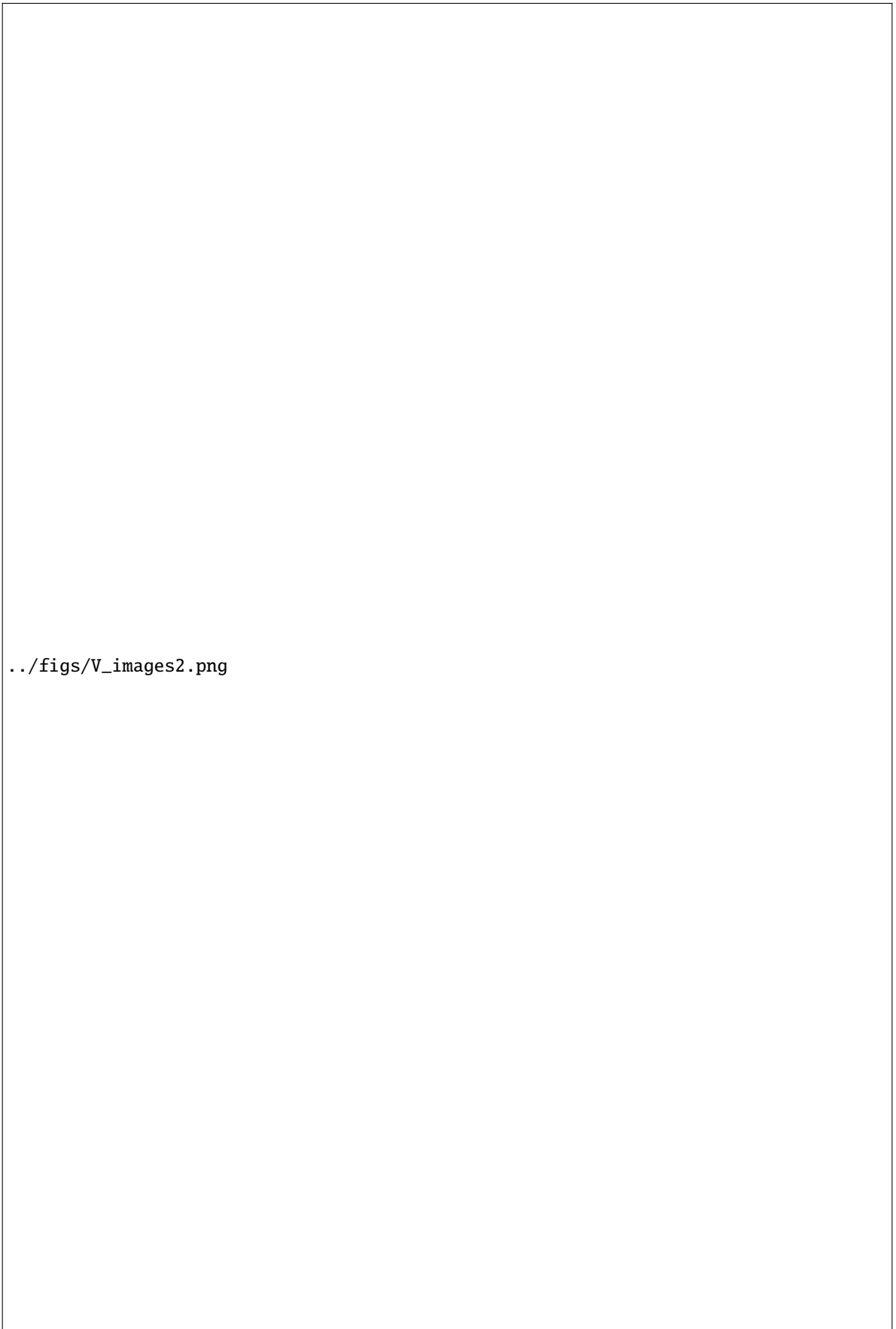


**Fig. 2.** Continued

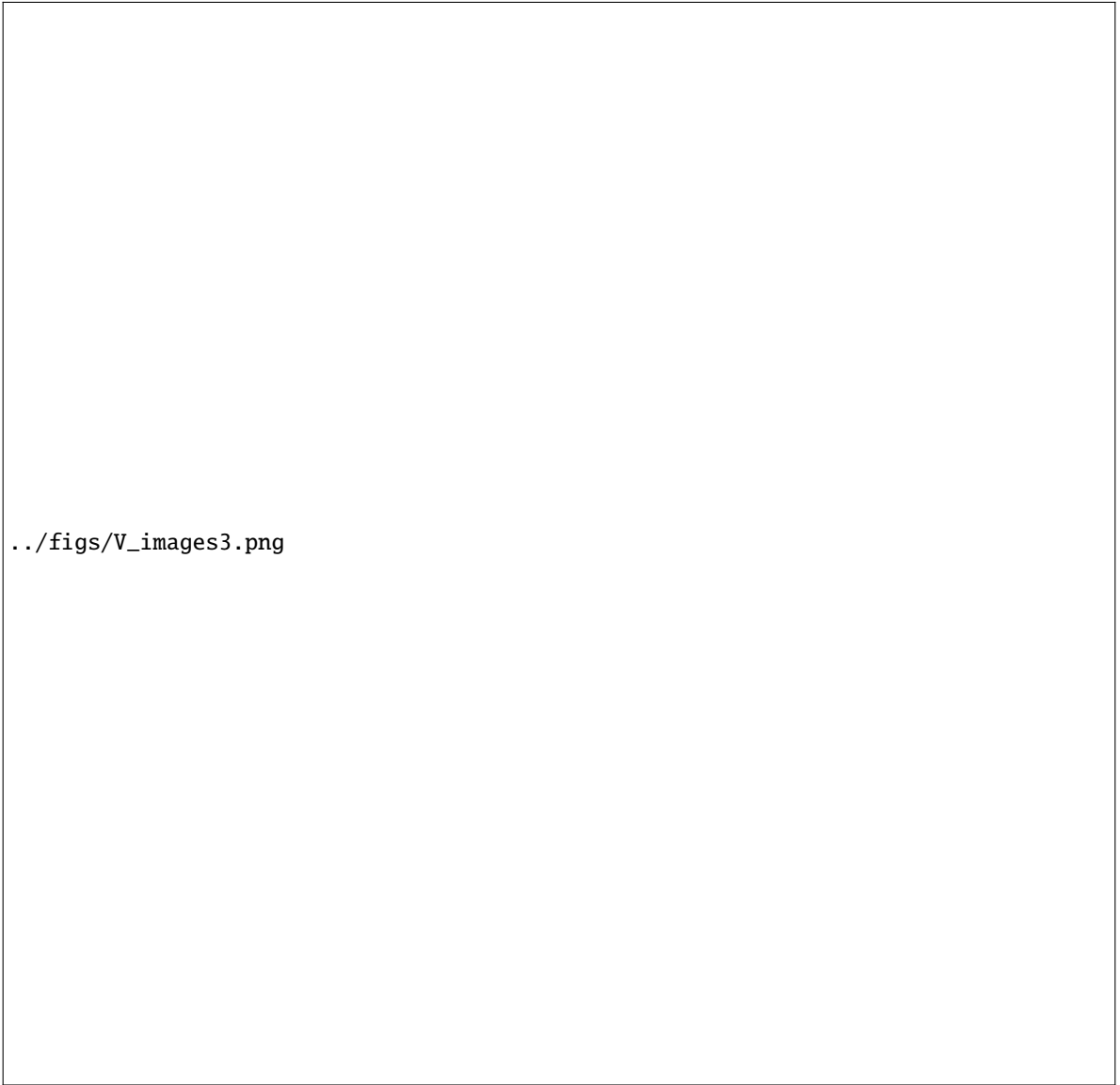


**Fig. 2.** Continued

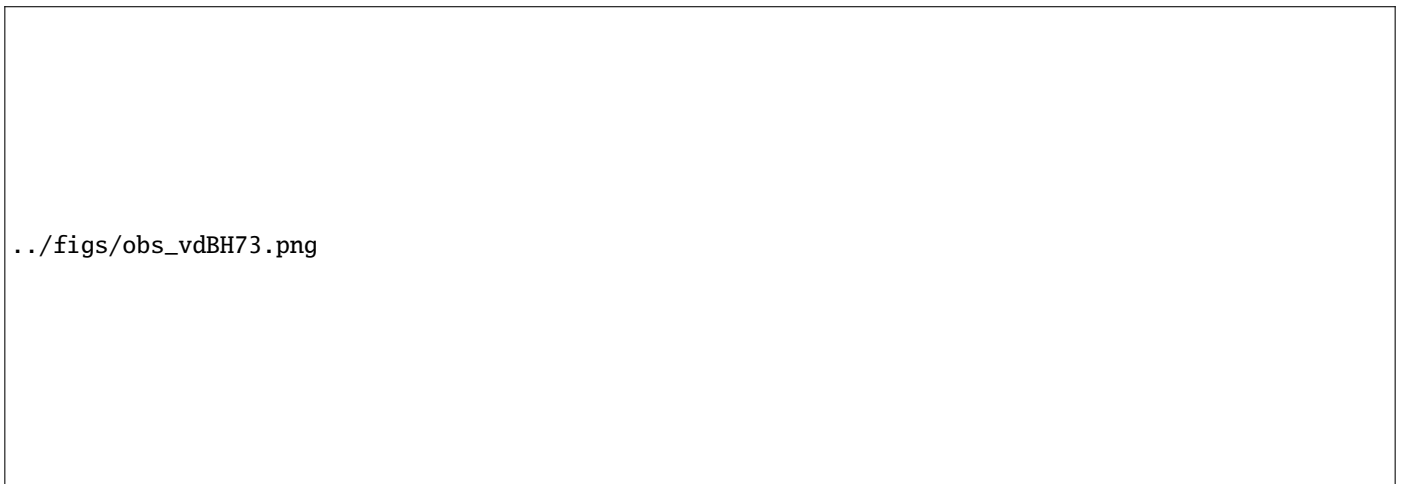


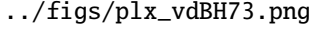
**Fig. 3.** From left to right: The  $V$  vs  $(B - V)$ ,  $V$  vs  $(V - I)$  and  $(B - V)$  vs  $(U - B)$  diagrams for all the stars observed in the region of van den Bergh-Hagen 73. The red dashed line in the two color diagram gives the position of the ZAMS (Aller et al. 1982). Inserts in the upper right corner in each diagram contain the number of stars included in the respective figure.

../figs/dmap\_vdbh73.png

**Fig. 4.** Left panel: The contour plot showing the position of the overdensity associated to vdBH 73. Green inner circle gives the cluster size while the two black dashed lines squares enclose the region used for ASteCA to estimate the field stars properties. Absolute coordinates in decimal format are indicated. The color scale at the right denotes the star number per square arcmin. Right panel: King profile is shown in dashed green line. The horizontal blue line is for the field mean star density. Vertical red line is set for the adopted cluster radius. The Poisson error ( $\sqrt{N}$ ) of each curve point is shown with a vertical black line.

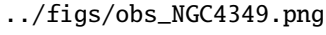
../figs/cmds\_vdbh73.png

**Fig. 5.** From left to right: The  $G$  vs  $(V - I)$ ,  $G$  vs  $(B - V)$  and  $(B - V)$  vs  $(U - B)$  clean diagrams after the removal by field interlopers made by ASteCA over vdBH 73. The color of each star reflects its membership probability. Corresponding values are in the color bar at the upper right corner in the  $G$  vs  $(V - I)$  diagram (left). Insert at the lower right corner in the  $G$  vs  $(V - I)$  diagram shows the number of stars used by ASteCA to compare with synthetic clusters. Insert in the mid panel includes the final results for metallicity,  $\log(\text{age})$ ,  $E_{(B-V)}$ , the corrected distance modulus, and the cluster total mass provided by ASteCA. The green continuous line in the three diagrams is a reference isochrone. In particular, the green line in the color-color diagram, mid panel, shows the most probable  $E_{(B-V)}$  value fitting found by ASteCA.



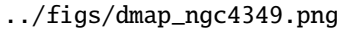
../figs/plx\_vdBH73.png

**Fig. 6.** Left panel: distribution of parallax for all stars with membership probabilities in the cleaned cluster region, as a function of the apparent magnitude  $G$  (vertical color scale is for the star membership probability) in vdBH 73. Horizontal bars are the parallax errors as given by Gaia DR2. The different parallax value fittings are shown by dashed lines of different colors (see text). The mid panel is a normalized comparison between the parallax distributions inside the cluster region (red line) and outside it (dashed black line). The frame at the right summarizes the distances in parsecs according to the Bayesian analysis ( $d_{Bayes}$ ) and ASteCA ( $d_{ASteCA}$ ) followed by the parallax corresponding value,  $Plx$ , and corrected distance modulus ( $\mu_0$ ). Both fittings are indicated by the vertical blue and green dashed lines. The last four text lines in the right panel are the AD values for  $Plx$ ,  $PM(\alpha)$ ,  $PM(\delta)$  followed by the corresponding  $p$ -values and, finally the combined  $p$ -value.



../figs/obs\_NGC4349.png

**Fig. 7.** Idem Fig. 3 for NGC 4349.



../figs/dmap\_ngc4349.png

**Fig. 8.** Idem Fig. 4 for NGC 4349.

../figs/cmds\_ngc4349.png

**Fig. 9.** Idem Fig. 5 for NGC 4349.

../figs/plx\_NGC4349.png

**Fig. 10.** Idem Fig. 6 for NGC 4349.

../figs/obs\_RUP87.png

**Fig. 11.** Idem Fig. 3 for RUP 87.



../figs/dmap\_rup87.png

**Fig. 12.** Idem Fig. 4 for RUP 87.

../figs/cmds\_rup87.png

**Fig. 13.** Idem Fig. 5 for RUP 87.

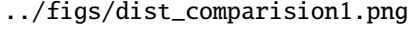
../figs/plx\_RUP87.png

**Fig. 14.** Idem Fig. 6 for RUP 87.



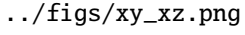
../figs/dist\_comparision2.png

**Fig. 15.** Top: AStECa (photometric) vs Bayesian (parallax) distances for the 10 clusters listed in Table 5. No bias correction applied to parallax data. Bottom: offset (AStECa - Bayes) for distances expressed as parallax. Colorbar to the right indicates  $\log(\text{age})$  values.



../figs/dist\_comparision1.png

**Fig. 16.** ASteCA (photometric) vs Bayesian (parallax) distances for the present sample, with bias corrections from Lindegren et al. (left), Schönrich et al. (center), and Xu et al. (right). Error bars are indicated along with the cluster names. The mean of differences between ASteCA and others distances is shown on top of the figures. Colorbar to the right indicates  $\log(\text{age})$  values.



../figs/xy\_xz.png

**Fig. 17.** The X-Y (upper panel) and X-Z (lower plane) projection of true and probable clusters in our sample. In the upper panel the thick grey line shows the trace of Carina arm according to (XXXX) while the dashed line in the lower panel is for the galactic equator. Clusters displaced from ASteCA position after adding systematic 0.1 mas to the parallaxes (red dots) are joined by a line. Empty squares enclose the youngest clusters in our list (see Table 5).

The thirteen clusters in this Appendix are ordered according to their right ascension, as shown in Table 1. The remaining three analyzed clusters were presented in Sect. 5.

## Appendix A: Ruprecht 85

Ruprecht 85 belongs to the south side of the Vela Constellation close to the border of the Carina region. This cluster appears in Fig. 2 as a slight increment in the stellar field towards the north part in the respective frame. The overall stars photometric diagrams as shown in Fig. A.1 do not show the presence of any cluster sequence but a vertical strip of stars emerging from a poorly populated stellar field above  $V = 14$  mag defined by disk stars.

The structural analysis performed by ASteCA yields a clean overdensity at the location of this object that appears subtending an almost circular area of 3 arcmins radius, Fig. A.2 left panel. As shown in the Fig. A.2 right panel, the RDP is well developed, scarcely noisy and with a star density five times above the background level. The photometric diagrams, CCD and CMDs of stars with membership probabilities above 0.74 and up to 1.0 shown in Fig. A.3 depict a main sequence sweeping 3.5 magnitudes. Intermediate probability members are found around the giant branch but we suggest that care should be taken with this fact. Combining structural evidences with evidences coming from the photometric diagrams we conclude that RUP 85 is a real entity. As for the cluster parameters of the best synthetic cluster fitting the observations it is found that:

- a) Like in the case of vdBH 73, RUP 85 is also placed in a region of moderate color excess. In fact the cluster has  $E_{(B-V)} = 1.06$  also entirely in line with a maximum  $E_{(B-V)}$  of 1.9 according to S&F2011.
- b) The free absorption distance modulus is 13.5 mag corresponding to a distance  $d = 5.01$  kpc.

The results from the Anderson-Darling test in Fig. A.4 applied to  $Plx$ ,  $PM(\alpha)$  and  $PM(\delta)$  indicate clearly that the cluster region and the surrounding background population come from quite different star populations. Therefore, the null hypothesis can be rejected.

We conclude that RUP 85 is a real open cluster over  $410 \times 10^6$  yr old.

## Appendix B: van den Bergh-Hagen 85

vdBH 85 appears in the sky slightly east of the center of the Vela constellation. The  $V$  chart in Fig. 2 shows a weak star concentration near the north side of the observed field extending a little bit to the south east. The photometric diagrams of the entire field of view is just a dispersed star distribution ending in a compact accumulation at  $(B - V) = 1$  and below  $V = 17$  mag approximately. Another clear feature in the two CMDs is a structure at  $V = 16$  and for  $1.2 < (B - V) < 1.7$  resembling a red clump.

ASteCA detected an overdensity very well detached from the stellar background reflected in the smooth RDP in Fig. B.2 contained in a circle 2.8 arcmins radius and more than five times the background density. Once the removal of field interlopers is done and the membership probabilities are established the two CMDs of all stars with probabilities above 0.58 show a short but evident

main sequence below  $G = 17$  mag. Three magnitudes above the cluster turn-off, at  $G = 14$  mag a handful of stars appear, possibly part of the bright end of the giant branch. Also at  $G = 14$  mag and almost located at the center of the CMDs, a couple of stars with MPs around 0.8 could be classified as blue stragglers associated to van den Bergh-Hagen 85. The comparison with the best fitting of a synthetic cluster throws the following characteristics for vdBH 85:

- a) the cluster is seen projected against a stellar field with moderate to low color excess. The best value corresponds to  $E_{(B-V)} = 0.28$  in correspondence with the maximum value of 0.45 stated by S&F2011.
- b) The free absorption distance modulus of vdBH 85 is 13.1 mag which implies a distance of 4.17 kpc from the Sun. This fact explains by itself the extreme weakness of cluster members.

The Anderson-Darling test results in Fig. B.4 suggest the null hypothesis can be safely rejected. In fact,  $Plx$ ,  $PM(\alpha)$  and  $PM(\delta)$  results from the Anderson-Darling test leave no doubt in the sense that cluster region and the surrounding comparison field come from quite different star populations.

We conclude that this object is a real cluster approximately  $7396 \times 10^6$  yrs old.

## Appendix C: van den Bergh-Hagen 87

Like RUP 85, vdBH 87 is seen toward the south of Vela Constellation close to the border with Carina. A weak grouping of stars placed towards the north of the frame is seen in Fig. 2. In turn, the CMDs in Fig. C.1 seem to reflect a typical star disk sequence up to  $V = 15$  mag approximately with an amorphous distribution at the bright end. The CCD is, on the other side, rather poor.

A stellar overdensity reaching  $\sim 20$  times the field star density is seen in Fig. C.2. The spatial structure of this overdensity suggests an elongation in right ascension and a RDP characterized by a very narrow density peak followed by a star coronal distribution at about 2 arcmins from the center. The clean CMDs in Fig. C.3 leave no doubt as for the nature of van den Bergh-Hagen 87 since inside this overdensity a robust and narrow cluster main sequence is evident. Its sequence extends for more than 5 mag in the CMDs, including stars with membership probabilities in the range from 0.80 to 1. The CCD on the other hand does not show a clear cluster sequence. The parameters of the synthetic cluster that best fits the real star distributions are:

- a) The color excess is  $E_{(B-V)} = 0.58$  indicating thus a moderate absorption in the cluster direction. In turn, this color excess value is below the maximum reddening  $E_{(B-V)} = 2.9$  computed in the region for S&F2011.
- b) The corrected distance modulus is 11.3 implying a distance of  $d = 1.9$  kpc. The cluster is not far from the Sun and this closeness explains the moderate color excess found.

The results of the application of the Anderson-Darling test in Fig. C.4 are coincident with what ASteCA have found. This is that cluster and field regions are quite different not only from the photometric perspective but also from a kinematic view.

In conclusion vdBH 87 is a real open cluster about  $320 \times 10^6$  years old.

../figs/obs\_RUP85.png

**Fig. A.1.** Idem Fig. 3 for RUP 85.

../figs/dmap\_rup85.png

**Fig. A.2.** Idem Fig. 4 for RUP 85.

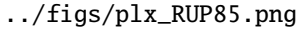
../figs/cmds\_rup85.png

**Fig. A.3.** Idem Fig. 5 for RUP 85.

## Appendix D: Trumpler 12

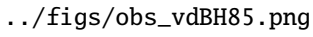
This object is placed in the west side of the Carina HII region where it appears as a sparse handful of bright stars in Fig. 2. The CMDs in Fig. D.1, including all stars in the region, show the following patterns: there is a wide grouping of stars below

$V = 18$  mag but to the right side of it, and also at this magnitude value, a narrow structure of stars up to  $V = 14$  mag slightly displaced to the blue side emerges. From  $V = 18$  mag a typical vertical galactic disk population rises too.



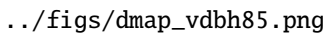
../figs/plx\_RUP85.png

**Fig. A.4.** Idem Fig. 6 for RUP 85.



../figs/obs\_vdBH85.png

**Fig. B.1.** Idem Fig. 3 for vdBH 85.

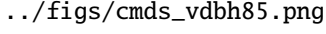


../figs/dmap\_vdbh85.png

**Fig. B.2.** Idem Fig. 4 for vdBH 85.

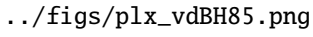
ASteCA detected a main overdensity and other less relevant ones shown in Fig. D.2. The reader can note a quite noisy RDP, a fact explained in part because at the peak of the RDP there is less than twice the density of the background. Under this condition is not an easy task to fix an appropriate radius for the overdensity. We tentatively adopt 3 arcmin radius as a reasonable compro-

mise. The membership probabilities in the zone of the overdensity range from 0.50 to 0.97 as indicated in Fig. D.3. We draw the attention to the fact that only 142 stars were detected inside the potential cluster zone. There exists a clear difficulty to separate field stars from cluster members, reflected in the noisy distribution visible in the CMDs. For  $G < 16$  mag some stars describe



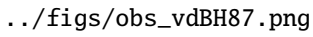
../figs/cmds\_vdbh85.png

**Fig. B.3.** Idem Fig. 5 for vdBH 85.



../figs/plx\_vdBH85.png

**Fig. B.4.** Idem Fig. 6 for vdBH 85.



../figs/obs\_vdBH87.png

**Fig. C.1.** Idem Fig. 3 for vdBH 87.

roughly a cluster main sequence. In particular some of them belonging to the tiny blue and narrow sequence detected easily in the diagrams of Fig. D.1 form part (including the turn-off stars) of the clean sequence between  $V = 12$  and  $V = 16$  mag seen in Fig. D.3. Comparison with synthetic clusters is still possible and the properties of the best fit achieved in the present case are the next:

- a) A color excess of  $E_{(B-V)} = 0.29$  is found for the best fitting. Since the maximum color excess provided by S&F2011 is 0.50 we found a precedent result and in case TR 12 is a real cluster it is placed in a zone of low absorption.
- b) The absorption free distance modulus becomes 12.4 representing a distance of 3.02 kpc. At such a distance and with



../figs/dmap\_vdbh87.png

**Fig. C.2.** Idem Fig. 4 for vdBH 87.

../figs/cmds\_vdbh87.png

**Fig. C.3.** Idem Fig. 5 for vdBH 87.

../figs/plx\_vdBH87.png

**Fig. C.4.** Idem Fig. 6 for vdBH 87.

low absorption it is reasonable to find a high background stellar density as seen in Fig. D.2. regions.

From the Anderson-Darling statistics shown in Fig. D.3 we see that proper motions for the cluster and for the field population belong to different samples. On the other hand, the parallaxes can not be safely separated into distinct stellar

The noisy profile that does not allow establishing a clear cluster extension and the poor main sequence requires us to be cautious. More deep photometry ( $(U - B)$  particularly) is needed to achieve a precise result as for the true nature of this object.

Meanwhile we conclude that TR 12 is a dubious cluster about  $800 \times 10^6$  years old.

## Appendix E: van den Bergh-Hagen 91

vdBH 91 is a potential cluster at the west side of Carina HII region, specifically near the northern border of this constellation with Vela. No relevant stellar structure appears in the *V* image of Fig. 2 but a common pattern of a galactic field star near the galactic plane. The overall CMDs in Fig. E.1 show a stellar sequence that, at first sight, resemble the usual diagrams for open clusters. In turn, the CCD is dominated by a tail of *F*- and *G*-type stars prolonged by red stars. It is noticed as well the presence of some reddened early type stars for negative ( $U - B$ ) indices.

ASteCA found two well separated stellar overdensity peaks in Fig. E.2 whose relevance in terms of stellar density is barely important since they include no more than three stars above the background density. The noisy RDP proves by itself the poverty of the entire field surveyed in term of star number. After some attempts looking for a cluster sequence we ask ASteCA to estimate the probabilities for stars inside an adopted radius of 3.6 arcmin shown in Fig. E.2 right. As seen in Fig. E.3 almost one hundred stars inside the circle associated to vdBH 91 were found in the CMDs with membership probabilities ranging from 0.43 to 0.80. It is interesting that most stars with lower probabilities outline a fictitious sequence below  $G = 16$  mag in these diagrams while stars with higher probabilities are scattered between the location of a probable main sequence and a giant stars branch. The absence of a cluster sequence combined with the poor and noisy overdensity are all against the reliability of this cluster. The Anderson-Darling test in Fig. E.4, right panel, is clear regarding the true nature of vdBH 91 since the high combined  $p$ -value indicates that the null hypothesis (cluster and field areas come from the same originating distribution) can not be reasonably rejected. This result is against the Kharchenko et al. (2005) findings who found that vdBH 91 is a cluster at 0.740 kpc, approximately  $160 \times 10^6$  yr old and affected by a mean color excess  $E_{(B-V)} = 0.08$ .

We conclude that vdBH 91 is a random fluctuation of the stellar foreground/background, and not a real entity.

## Appendix F: Ruprecht 88

RUP 88 is another potential cluster south of the Carina HII region. Like other objects in this paper no obvious stellar grouping is perceived in the *V* image of Fig. 2. The overall star CMDs in Fig. F.1 show a scattered star distribution above  $V = 16$  mag. From this magnitude down the common pattern of galactic disc stars takes place in the CMDs. The CCD in Fig. F.1 suggests that no blue and therefore young star is present in the region of RUP 88. Just at  $0.2 < (B - V) < 0.8$  we see a handful of stars that could be reddened late of late *B*-types or *A - F*-type stars. The remaining of this diagram is a trace composed by *A*- to *M*-type stars.

As with other clusters in the present sample, when the spatial distribution of stars in the frame is analyzed no clear star overdensity appears in the location where RUP 88 is supposed to exist. In fact, the contour plot in Fig. F.2, left panel, shows a poor star number enhancement from south west to northeast of the

frame extending north west. Given the difficulties to state the position of the cluster center (if it exists) we ask ASteCA to inspect the region encircled in green in Fig. F.2, where a reasonable density profile could be found. The RDP is still noisy because of a rather poor star number contained between the assumed cluster limits. If we look at Fig. F.3, in the CMDs, only 38 stars with probabilities ranging from 0.01 to 0.71 remain inside the adopted cluster region, quite low membership probability values perhaps reflecting the trouble to set aside the cluster region from the field region. The findings in the three photometric diagrams in Fig. F.3 confirm this point as only an amorphous distribution of stars scarcely resembling a cluster main sequence can be seen.

The Anderson-Darling test in Fig. F.4, right panel is unable to separate the cluster population from the one from the field region, for all the three explored dimensions. The combined  $p$ -value for proper motions and parallaxes is large, suggesting that both samples do not come from the same population. The necessary requirement that there is a reasonable main sequence is absent and, combined with this result, precludes concluding that RUP 88 is a true cluster.

## Appendix G: van den Bergh-Hagen 92

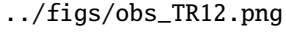
Placed south of Vela, near the eastern border with Carina, vdBH 92 is a relevant handful of bright stars as seen in the *V* image of Fig. 2. The CMDs and CCD for all stars in the region, as shown in Fig. G.1, depict a narrow star sequence with some scatter at their respective bright ends. Particularly the CCD shows, not far from the intrinsic line, a group of *F*- and *G*-type stars and another group of stars below the intrinsic line that could be *B*- and *A*-type stars displaced by the reddening effect.

ASteCA analysis in Fig. G.2 revealed the presence of a well isolated star overdensity rising above the field stars density of about 4 stars per square arcmin. We identify this overdensity with vdBH 92. Notwithstanding the noisy RDP the limits of the overdensity can be well established. As indicated in Fig. G.3 few stars have been found inside the cluster limits with membership values from 0.81 to 0.97. Despite such a low number of members, a 7 magnitude extended cluster main sequence is been found. The comparison with synthetic clusters made by ASteCA yields:

- the best fitting of a synthetic cluster to the clean data in Fig. G.3 indicates a color excess of  $E_{(B-V)} = 0.66$ . Since the maximum color excess provided by S&F2011 is 2.34 for this zone we conclude that most of the absorption is produced behind the position of van den Bergh-Hagen 92. This object is therefore placed in front of a strong absorption region.
- The absorption free distance modulus becomes 11.5 what places van den Bergh-Hagen 92 at a distance of  $d = 2$  kpc.

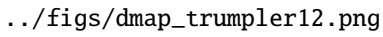
By applying the Anderson-Darling test it is noticed that the parallax distributions for stars inside and outside the cluster boundaries are not different from each other as indicated in the right panel of Fig. G.4. However, proper motions are quite different in both regions. We associate this last finding with the presence of a well defined overdensity that, in turn, shows a reasonable and extended cluster main sequence to conclude that both samples come from different populations.

All this together confirm the true nature of vdBH 92. This is a young cluster  $83 \times 10^6$  years old.



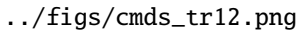
../figs/obs\_TR12.png

**Fig. D.1.** Idem Fig. 3 for TR 12.



../figs/dmap\_trumpler12.png

**Fig. D.2.** Idem Fig. 4 for TR 12.



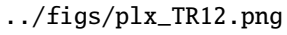
../figs/cmds\_tr12.png

**Fig. D.3.** Idem Fig. 5 for TR 12.

## Appendix H: Trumpler 13

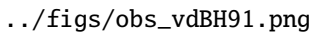
TR 13 is a weak object also at the south west of the Carina HII region, seen as a diffuse but extended star accumulation near the center of the  $V$  image in Fig. 2. The two CMDs in Fig. H.1 show an uncommon pattern: we see that above  $V = 17.5$  mag the star

sequence splits into two branches with one of them extending to the bluest side while other branch follows the common representation of galaxy disc stars. In the CCD the situation is the same: a wide and reddened band of potential  $B$ -type stars is placed for  $(B - V) < 0.45$  and for  $-0.25 < (U - B) < 0.5$  with a few more stars at negative  $(U - B)$  index while another



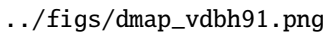
../figs/plx\_TR12.png

**Fig. D.4.** Idem Fig. 6 for TR 12.



../figs/obs\_vdBH91.png

**Fig. E.1.** Idem Fig. 3 for vdBH 91.



../figs/dmap\_vdbh91.png

**Fig. E.2.** Idem Fig. 4 for vdBH 91.

strip of stars goes from the characteristic place for *F*-type stars extending to the red tail including probable giant stars.

Fig. H.2 indicates that ASteCA found a spatially extended overdensity mostly elongated north-south, which, at its peak is nearly 5 times above a mean field stellar density of 12 stars per

square arcmin. Given the shape and extension of the overdensity we adopted a formal radius 3.7 arcmin and asked ASteCA to compute the membership probabilities for those stars inside the area. Fig. H.3 shows that after the removal of field interlopers, almost 180 stars with membership values from 0.04 to 0.97 are left composing a narrow cluster main sequence extending for

../figs/cmds\_vdBH91.png

**Fig. E.3.** Idem Fig. 5 for vdBH 91.

../figs/plx\_vdBH91.png

**Fig. E.4.** Idem Fig. 6 for vdBH 91.

../figs/obs\_RUP88.png

**Fig. F.1.** Idem Fig. 3 for RUP 88.

more than 6 magnitudes. Consequently, when comparing with synthetic clusters the results yield:

most of the absorption is produced behind the position of TR 13.

- a) A color excess of  $E_{(B-V)} = 0.55$  is found for the best fitting of a synthetic cluster. Since the maximum color excess provided by S&F2011 is 1.94 it is reasonable to conclude that
- b) The absorption free distance modulus of TR 13 is estimated to be 13.0 mag, placing it at a distance of 3.98 kpc from the Sun.

../figs/dmap\_rup88.png

**Fig. F.2.** Idem Fig. 4 for RUP 88.

../figs/cmds\_rup88.png

**Fig. F.3.** Idem Fig. 5 for RUP 88.

../figs/plx\_RUP88.png

**Fig. F.4.** Idem Fig. 6 for RUP 88.

The Anderson-Darling statistics in Fig. H.4, right panel, confirm the photometric results. In fact, cluster area and the surrounding field region possess quite different properties.

Although not particularly large, probabilities for stars inside the overdensity confirm the true nature of this object since the over density and the density profile are followed by a very well

defined and extended photometric counterpart. All these facts combined with the results from the Anderson-Darling test are self-consistent, so that we are confident that TR 13 is a young cluster  $27 \times 10^6$  years old.

../figs/obs\_vdBH92.png

**Fig. G.1.** Idem Fig. 3 for vdBH 92.

../figs/dmap\_vdbh92.png

**Fig. G.2.** Idem Fig. 4 for vdBH 92.

../figs/cmds\_vdbh92.png

**Fig. G.3.** Idem Fig. 5 for vdBH 92.

## Appendix I: van den Bergh-Hagen 106

This cluster is placed at the south-east of the Vela constellation. The not so dense stellar field where it is placed has no relevant features except a few moderately bright stars as shown in Fig. 2. The CMDs shown in Fig. I.1 represent typical photometric

features structures of galactic fields with no cluster inside. As for the CCD in the same figure it shows a reduced number of stars below the intrinsic line (probably reddened late *B*- and *A* types) and a tail of stars from of late *F*-types to *M*-type stars –some of them probably giant- at the red end. ASteCA spatial analysis found some star clumps as seen in Fig. I.2, left panel.



../figs/plx\_vdBH92.png

**Fig. G.4.** Idem Fig. 6 for vdBH 92.

../figs/obs\_TR13.png

**Fig. H.1.** Idem Fig. 3 for TR 13.

../figs/dmap\_trumpler13.png

**Fig. H.2.** Idem Fig. 4 for TR 13.

We focus the attention on the main one at the very center of the frame, since here we see the highest overdensity peak with 4 times more stars than at the mean stellar background density of 7 stars per square arcmin approximately. We assume that most of stars in vdBH 106 must be included there so the cluster parameters should be well established. It is a fact that the RDP ap-

pears not well defined since it reflects the irregular and poor star density even inside the zone selected to investigate the cluster parameters. Only 87 stars have been found inside this area. The membership values for stars inside the putative cluster position range from 0.23 to 0.91. However, those stars having probabilities near the maximum values in this region still outline a cluster

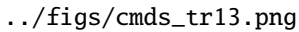


**Fig. H.3.** Idem Fig. 5 for TR 13.

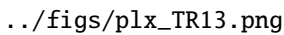


**Fig. H.4.** Idem Fig. 6 for TR 13.

main sequence that can be fitted with a synthetic cluster which yields the following parameters:

- a) A color excess of  $E_{(B-V)} = 0.30$  has been found to affect the cluster. This value is well in line with the maximum color excess provided by S&F2011,  $E_{(B-V)} = 0.57$  in this direction.
- b) The absorption free distance modulus of vdBH 106 was found to be 14 mag, putting the cluster at a distance of  $d = 6.3$  kpc from the Sun.

In this region we found from the application of the Anderson-Darling test that the parallax and proper motion distributions seem to belong to the same originating distribution, as seen in Fig. I.4. Indeed, the large combined p-value makes the rejection of the null hypothesis difficult, since the probability of erroneously rejecting it is around 22% (capped at that maximum value by the Python package used to estimate it).

Despite a trace of a sequence belonging to a typical old cluster is noticeable in Fig. I.3, we are cautious as to confirm its nature. Clearly deeper photometric observations (particularly in the  $U$  filter) are needed. Meanwhile and under the assumption we are facing a true object van den Bergh-Hagen 106 could be an old open cluster around  $9705 \times 10^6$  years old (the oldest in our sample).

## Appendix J: Ruprecht 162

Placed to the south east of the Carina HII region, the  $V$  image of the region in Fig. 2 where the cluster is supposed to exist shows a moderate number of stars resembling a star grouping placed at the north-west in the frame. At first sight the CMDs in Fig. J.1 for the overall stars look as if a cluster main sequence is emerging from the trace of the disk star distribution. In the same figure, right panel, the CCD splits into two star groups: one of them is mostly placed below the intrinsic line for  $0.0 < (B - V) < 0.8$  and resembles a strip of reddened blue stars (including early and late  $B$ -types and, perhaps, some  $A$ -type stars); the other group shows a distribution of  $F$ - to  $M$ -type stars strongly affected by reddening in appearance.

ASteCA detected an extended and irregular region at the north-west of the frame in Fig. J.2 (where the cluster is supposed to lie). Given the difficulties to set a clear overdensity we decided to focus the attention on the zone encircled in green in Fig. J.2, left panel. The background mean star density is over 12 stars per squared arcmin and, at the most, the overdensity is just 20 stars at the maximum. This produces unavoidably a noisy RDP (it is hard to establish a meaningful radius and there is a quite irregular star distribution across the zone). The CMDs and CCD in Fig. J.3 after the removal of field interlopers tell us that stars in the adopted cluster region have membership probabilities in the

../figs/obs\_vdBH106.png

**Fig. I.1.** Idem Fig. 3 for vdBH 106.

../figs/dmap\_vdbh106.png

**Fig. I.2.** Idem Fig. 4 for vdBH 106.

../figs/cmds\_vdbh106.png

**Fig. I.3.** Idem Fig. 5 for vdBH 106.

range 0.03 to 1.0. Stars above  $G = 16$  mag have membership values over 0.6 but are all scattered in the range  $0.2 < (B - V) < 2$ . When one looks closely at the right and left panels in Fig. J.3, a small group of stars with the largest memberships appear at the low mass end. The cleaned CCD, Fig. J.3 mid panel, leaves a blue sequence of stars suffering some internal color scatter fol-

lowed by a tail of  $F$ - to  $K$ -type stars. Therefore this object could be more extended than supposed. ASteCA found the best fitting with a synthetic cluster with the following properties:

- a) The color excess affecting the cluster is  $E_{(B-V)} = 0.47$  inside the values given by S&F2011 who estimate  $E_{(B-V)} = 1.07$  at maximum and 0.91 at minimum.

../figs/plx\_vdBH106.png

**Fig. I.4.** Idem Fig. 6 for vdBH 106.

- b) The absorption free distance modulus is 12.3 mag corresponding to a distance of  $d = 2.9$  kpc.

Anderson-Darling statistical test results are shown in Fig. J.4, right panel. Parallaxes and proper motions  $PM(\alpha)$  and  $PM(\delta)$  in the location of RUP 162 and the surrounding field region do not seem to be different enough from each other as to be efficiently disentangled.

Although weak enough the presence of a probable main sequence in the panels of Fig. J.3, make us cautious leaving some chance for RUP 162 to be a true and young cluster about  $31 \times 10^6$  yr old. An additional reinforcement as for the hypothetical true entity of this young object is the existence of a sudden gap along the main sequence at  $G = 16.5$  mag and the presence of high probability stars at the red side resembling traces of a pre-main sequence. Certainly we are just speculating on this fact so that more and deeper observations are needed to arrive to a concluding result for RUP 162.

## Appendix K: Lynga 15

This is an intriguing object placed in Centaurus, south west between Crux and the east border of Carina. More specifically, Lynga 15 is about  $1^\circ$  north-east of the star formation region SFR293.64-1.41 (Avedisova 2002). Like in many other cases already shown in the  $V$  images in Fig. 2 this region does not show, at first glance, any prominent stellar feature though some stars are bright enough as to attract attention to this place. Maybe the detection of a planetary nebula (PN Hf 69, reference!) is another reason to draw the attention. However, the overall CMDs and CCD shown in Fig. K.1 are quite surprising since both CMDs depict an extended sequence (from  $V = 8$  down to  $V = 16$  mag) emerging toward the left side of the main disc population trace. In the same figure, right panel, the CCD shows a strip of blue stars ( $0.6 < (B - V) < 0.0$ ) accompanied by other, probable reddened early type stars, placed above  $(U - B) = 0.0$ . The picture seen in the three panels of Fig. K.1 induces to think of Lynga 15 as a quite young open cluster.

In turn, ASteCA analysis of the spatial structure found an extended and irregular star overdensity reaching few more than 20 stars per square arcmin. After many attempts to look for the place where the star membership probabilities reach the highest values we adopted a 4.6 arcmin radius and set the potential

cluster center in the literature coordinates as indicated in Fig. K.2, left panel. In this place, the RDP displays a 10 stars per squared arcmin peak above the stellar field density, as seen in the right panel of Fig. K.2. However, even in this position ASteCA yields a conflictive result since star membership probabilities go from 0.3 to 0.94 but as seen in Fig. K.3, left and right panels, a probable cluster main sequence mostly composed by low probability stars appears below approximately  $G = 17.5$  mag. Above this visual magnitude the main sequence vanishes and just a handful of stars with large probability values, scattered in color index and magnitudes, takes place a full magnitude above. This is, no upper cluster main sequence is evident in the clean CMDs. It draws the attention that the CCD in the mid panel of Fig. K.3 contains a few blue stars with no counterpart in the CMDs. This could be explained this way: all across the surveyed region there are blue stars (see the overall CCD in Fig. K.1) composing a sort of Blue Plume in the respective CMDs and just by chance some blue stars also appear in the potential cluster region after ASteCA analysis (mid panel Fig. K.3). It could be possible yet that Lynga 15 is an extended open cluster (even larger than the size of our frame) but the presence of the huge star gap above  $G = 17.5$  mag is unexplainable in a CMD from a statistical point of view. In our opinion and from a photometric and spatial point of view Lynga 15 is not an open cluster. The application of the Anderson-Darling test inform us that the properties of stars inside the adopted cluster radius and outside of it are similar, with a probability above 6% of mistakenly rejecting the null hypothesis (i.e.: not low enough to reject it).

We conclude that Lynga 15 is not a true cluster but a superposition of blue stars at several distances along the line of sight (see that this is highly probable). This is not odd at all since this object is not far from the galactic equator and it is close enough to SFR293.64-1.41 as indicated above; so, it is probable that blue stars are seen along the direction to this potential cluster.

## Appendix L: Loden 565

Placed toward the west side of the Crux constellation the  $V$  image in Fig. 2 of Loden 565 does not show any evident star grouping. Inspection of the CCD and CMDs in Fig. L.1 only suggests the presence of a dispersed star group down to  $V = 15 - 16$  mag approximately. From this magnitude down the overall CMDs show the common pattern of galactic disc star

../figs/obs\_RUP162.png

**Fig. J.1.** Idem Fig. 3 for RUP 162.

../figs/dmap\_rup162.png

**Fig. J.2.** Idem Fig. 4 for RUP 162.

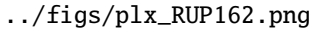
../figs/cmds\_rup162.png

**Fig. J.3.** Idem Fig. 5 for RUP 162.

population and nothing relevant can be seen in the CCD in the mid panel of Fig. L.1, but a modest handful of probable slightly reddened late blue stars for  $(B - V) < 0.6$ .

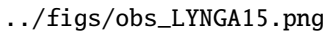
ASteCA found an irregular overdensity at the north-west corner of the frame as seen in Fig. L.2, left panel. This is the

only region across the entire field where a sudden increase in the star number per area unit is noticeable showing a 25 stars per squared arcmin peak at its maximum in Fig. L.2, right panel. When looking for membership probabilities only a small number of 58 stars remain inside the adopted radius with probabilities ranging from 0.52 to 0.65, quite low indeed.



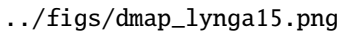
../../figs/plx\_RUP162.png

**Fig. J.4.** Idem Fig. 6 for RUP 162.



../../figs/obs\_LYNGA15.png

**Fig. K.1.** Idem Fig. 3 for Lynga 15.



../../figs/dmap\_lynga15.png

**Fig. K.2.** Idem Fig. 4 for Lynga 15.

Still at such low values a weak lower main sequence appears in the CMDs in Fig. L.3 while other stars with larger values are scattered along above  $G = 16$  mag. Notice that none of the stars that occupy the CCD of Fig. L.1 (right panel) with  $0 < (B - V) < 0.6$ , with some chances to be reddened early type stars, remain inside the adopted area after ASteCA's

membership analysis. The stars that ASteCA identified inside the adopted radius could be members of an old group but we conclude that the photometric evidences are not conclusive at all. More extended and deeper observations are necessary. Previous estimates of the cluster parameters found for Loden 565 can be found in Kharchenko et al. (2005). These authors

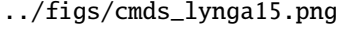


**Fig. K.3.** Idem Fig. 5 for Lynga 15.

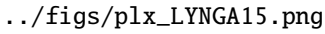


**Fig. K.4.** Idem Fig. 6 for Lynga 15.

concluded that Loden 565 is a moderately young cluster placed at a distance of  $d = 0.650$  kpc, affected by a mean reddening  $E_{(B-V)} = 0.2$  and a little older than  $10^8$  yrs. The Kharchenko et al. (2005) atlas shows a poor fitting to a very sparse available data. In addition, when inspecting the results from the Anderson-Darling test in the right panel of Fig. L.4, it becomes evident that the cluster region is indistinguishable from the stellar background in terms of parallax and proper motion distributions, exactly as the clean CCD and CMDs show in Fig. L.3.

In conclusion, Loden 565 is more probably a stellar fluctuation.

## Appendix M: NGC 4230

This object belongs to the Centaurus region immediately close to the upper border of Crux. The  $V$  image in Fig. 2 shows that we are facing just a modest star grouping near the high proper motion star HD 106826 (is this of some value?) with 8.8 mag. Nothing relevant is appreciable in the  $V$  image of the inspected zone except the star already mentioned. A highly scattered and diffuse star distribution resembling a boring galactic disc stellar pattern appears in the overall CCD and CMDs in the panels of Fig. M.1.

The spatial inspection performed by ASteCA detected a group of small stellar overdensities surrounding the central prominence as shown in Fig. M.2, left panel. The peak of the central overdensity shows that the number of stars per area unit is three times the mean of the background, and the respective RDP in the right panel of Fig. M.2 suggests a 2.7 arcmin radius. However, ASteCA yielded a frustrating result in terms of what it is expected for a real cluster when analyzing the stellar properties inside and outside the overdensity. In fact, only 44 stars remain inside the limits we adopted for NGC 4230 whose membership probability values range from 0.40 to 0.87. The synthetic cluster fit is found for the low mass stars with the smaller MP values. At this membership level there is no way to confidently separate the stellar population into those objects belonging to a real open cluster and those others belonging to the stellar field. The CCD and CMDs of these 44 stars in Fig. M.3 reflect the physical situation since no main sequence is evident at all. At most, there is a sort of badly defined giant star sequence whose meaning is dubious because there is no trace of a main sequence. The comparison with synthetic clusters performed by ASteCA fitted mainly a group of stars with low brightness, as shown in the CMDs of Fig. M.3. This cluster is analyzed in Tadross (2011) where the authors find an old 1.7 Gyrs cluster (similar to our result of 4.3 Gyrs) but at a much closer distance (1445 pc versus our result of about 11000 pc) Therefore the studies do not coincide in the nature of this



../figs/obs\_LODEN565.png

**Fig. L.1.** Idem Fig. 3 for Loden 565.

../figs/dmap\_loden565.png

**Fig. L.2.** Idem Fig. 4 for Loden 565.

../figs/cmds\_loden565.png

**Fig. L.3.** Idem Fig. 5 for Loden 565.

supposed cluster.

different for stars outside the cluster region.

Results for the distribution of parallax values and proper motions for the cluster and field regions are shown in Fig. M.4, right panel. We see that the Anderson-Darling statistics reveals that the parallax and proper motions distributions are very

The lack of a well-defined photometric sequence proper of an open cluster as demonstrated in Fig. M.3 together with the results from the statistical comparison is enough argument to ex-

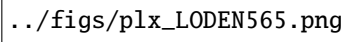


**Fig. L.4.** Idem Fig. 6 for Loden 565.

clude NGC 4230 as a true open cluster, becoming most probably  
a random fluctuation of the stellar field.

../figs/obs\_NGC4230.png

**Fig. M.1.** Idem Fig. 3 for NGC 4230.

../figs/dmap\_ngc4230.png

**Fig. M.2.** Idem Fig. 4 for NGC 4230.

../figs/cmds\_ngc4230.png

**Fig. M.3.** Idem Fig. 5 for NGC 4230.

../figs/plx\_NGC4230.png

**Fig. M.4.** Idem Fig. 6 for NGC 4230.